September Melt at the Summit in Greenland

An Attribution Study of the September 2022 Extreme Melt Event and a Projection of Future Events

MSc Thesis

Nadine Tiessen

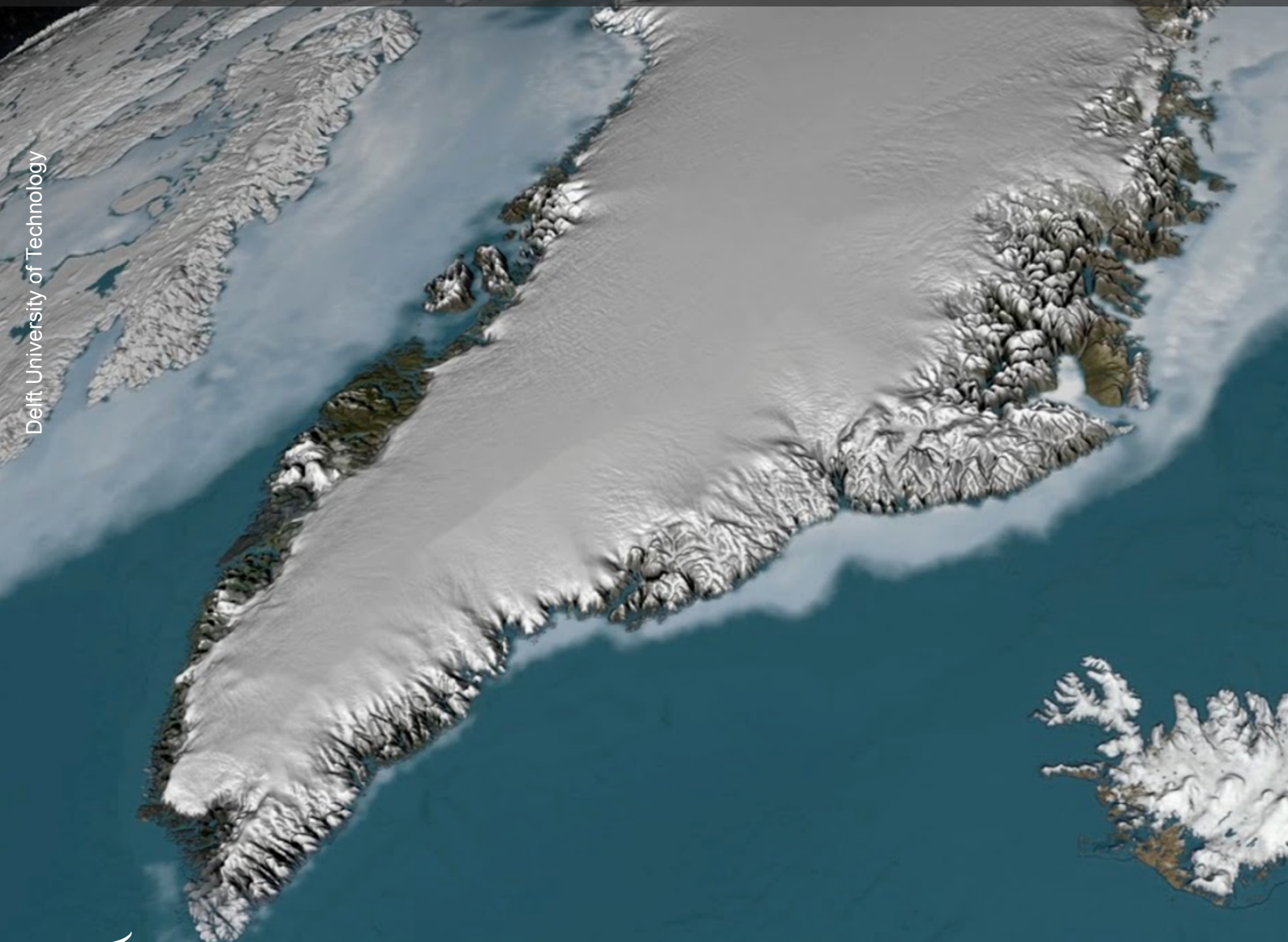

Delft University of Technology

TU Delft

September Melt at the Summit in Greenland

An Attribution Study of the September 2022 Extreme Melt Event and a Projection of Future Events

by

Nadine Tiessen

to obtain the degree of Master of Science
at the Delft University of Technology,
to be defended publicly on Monday October 9, 2023 at 13:45.

Student number:	4574931	
Project duration:	September 2022 – September 2023	
Thesis committee:	Dr. ir. B. Wouters,	TU Delft, daily supervisor
	Dr. M. A. Schleiss,	TU Delft
	Dr. M. Vizcaino,	TU Delft

An electronic version of this thesis is available at `http://repository.tudelft.nl/`.

Cover image: Snapshot from a movie showing the 3D map of Greenland created by NASA. Credits: NASA Goddard's Scientific Visualization Studio

TU Delft

Abstract

In September 2022, Greenland experienced an extraordinary late-season melt event, characterized by temperatures exceeding the melting point at Summit Station for the first time on record and surface melt appearing across one-third of the ice-sheet.

This thesis investigates extreme melt events at the Summit in Greenland, focusing on the attribution of the September 2022 extreme melt event to human-induced climate change. The study combines observational data and climate model simulations to assess the influence of climate change on these events and project their likelihood in the future. The research involved identifying melt events in observational and model data. Subsequently, melt-event probability ratios were calculated between the pre-industrial, current, and future climates. These ratios were synthesized to form an attribution statement and provide insights into future scenarios.

The study reveals that melt events in any month at the Summit in Greenland have become 20 times more likely in the current climate compared to the pre-industrial climate. This increase in likelihood of melt events in any month is significant and can be attributed to human-induced climate change. However, for melt events specifically in September, although unprecedented in pre-industrial and recent times, no significant increase is found due to a lack of data. Definitive conclusions are expected with more data. Projections based on climate models indicate a substantial rise in future melt event probabilities, reaching up to a 46% chance of Summit melt in September and a 83% chance throughout the remainder of the year.

The findings suggest that, while the September 2022 event cannot definitively be attributed to climate change, it highlights the increasing likelihood of such events and their potential impact on sea levels. However, the analysis carries inherent uncertainties due to limited historical and climate model data usage and limited consideration of atmospheric river circumstances. Despite these challenges, these insights contribute to enhancing our understanding of extreme melt events and, in turn, inform the formulation of future climate mitigation and adaptation strategies.

Preface

This thesis represents my final work for obtaining a master's degree in Civil Engineering, specializing in Geoscience and Remote Sensing. It marks the end of my journey as a student at the TU Delft, during which I acquired invaluable experiences and knowledge. The process of researching and writing this thesis has been enlightening both on an academic and personal level. I learned about the complexities of Greenland, observations and climate models, while also discovering the importance of maintaining flexibility and openness to adjusting the research trajectory when circumstances demanded it. Studying Greenland, a region profoundly impacted by climate change, exposed me daily to the harsh realities of human actions and their negative consequences. It is the hope for a better future and the belief that research can contribute to positive change that serve as the driving force behind this thesis.

I would like to take a moment to acknowledge the individuals and factors that have contributed to the realization of this thesis. First and foremost, I would like to express my gratitude to my main supervisor and chair of the assessment committee, Bert Wouters. Your guidance and engagement have been indispensable in making this thesis possible. Thank you for all the weekly meetings during which you provided valuable discussions and feedback. Additionally, I wish to thank my other supervisors and committee members, Marc Schleiss and Miren Vizcaino. Marc, your incisive questions and constructive feedback have elevated the quality of my thesis. Miren, I am grateful for your willingness to assist whenever I needed guidance, as well as your well-thought through answers to my questions.

I cannot overstate my appreciation for my fellow students, especially those who worked alongside me in room 3.36. I am thankful for the countless coffee breaks, much-needed discussions, and the supportive atmosphere we fostered. I would be remiss if I did not acknowledge my family, friends, and partner for their unwavering support. Their willingness to review my work when requested and offer reassuring words have been invaluable throughout this journey. Last but not least, I would like to acknowledge the assistance of ChatGPT in rewriting certain parts and conducting a grammar check of the report.

Nadine Tiessen
Delft, September 2023

Nomenclature

Abbreviations and Symbols

AOI	Area Of Interest
AR	Atmospheric River
AWS	Automatic Weather Station
CESM HR(LR)	Community Earth System Model High Resolution (Low Resolution)
CESM LE	Community Earth System Model Large Ensemble
CI	Confidence Interval
CMIP5(6)	Coupled Model Intercomparison Project Phase 5(6)
ECMWF	European Centre for Medium range Weather Forecasts
ERA-5(I)	ECMWF Reanalysis fifth generation (interim)
GC-Net	Greenland Climate Network
GCM	Global Climate Model/General Circulation Model
GEOSummit	Greenland Environmental Observatory
iHESP	international Laboratory for High-Resolution Earth System Prediction
IVT	Integrated water Vapor Transport
MAR	Modèle Atmosphérique Régional
MERRA(2)	Modern-Era Retrospective analysis for Research and Applications (Version 2)
NCAR	National Centre for Atmospheric Research
NRT	Near Real Time
NSF	U.S. National Science Foundation
NSIDC	National Snow & Ice Data Center
p	Probabillity
PI	Pre-Industrial
PM	Passive Microwave
PR	Probabillity Ratio
RACMO	Regional Atmospheric Climate MOdel
RCM	Regional Climate Model
RCP8.5	Representative Concentration Pathway 8.5
SMB	Surface Mass Balance
WWA	World Weather Attribution collaboration

Contents

1

Introduction

Background and significance

In September 2022 a very unusual late-season melt event occurred in Greenland (NSIDC, 2022). From 2-5 September a heatwave hit Greenland, resulting in a large melt event during which 36% of the ice sheets' surface was melting, a substantial peak in meltwater runoff occurred and above-freezing temperatures were recorded (Mote, 2014). This melt record is unprecedented in the 44-year-long satellite-era and the runoff ranks among the 10 highest runoff days since 1950 (NSIDC, 2022).

Extreme melt events contribute to the melting of the Greenland ice sheet, which has profound implications for global sea levels (Nghiem et al., 2012) (Oppenheimer et al., 2019). Over the past decade, Greenland has faced several extreme events which greatly enhanced the surface mass loss of the Ice Sheet (Hofer et al. (2017), Bevis et al. (2019), Tedesco and Fettweis (2020)). Also extreme melt events in the future can contribute to additional mass loss, leading to approximately 0.5m or 14% extra sea level rise by 2300 (Beckmann and Winkelmann, 2023). The Greenland Ice Sheet, with its potential to contribute to a 7-meter sea level rise, stands as a pivotal factor in global-mean sea level rise (Morlighem et al., 2017). The implications of rising sea levels on people's lives are profound, particularly for coastal communities (Oppenheimer et al., 2019). These impacts encompass lateral and inland migration, as well as the loss of functionality and biodiversity in coastal areas.

Understanding these events is becoming increasingly crucial, as extreme events like these may become increasingly common with progressing global warming. The Arctic region, including Greenland, has experienced a pronounced temperature increase, with near-surface air temperatures rising at a rate three times higher than the global mean between 1971-2019 (AMAP, 2021). With the increase in mean temperature, the occurrence of extremely high temperatures also increases. The increase in extremely high temperatures is more than the increase in mean temperature due to the non-linear relation between means and extremes (van der Wiel and Bintanja, 2021). An increase in hot extremes has already been observed since 1950 and attributed to climate change (Arias et al., 2021). The increase in extremely high temperatures can result in (extreme) melt events occurring more frequently and with greater intensity in Greenland. A study into the frequency and intensity of extreme melt events in the future as well as the attribution of past events to anthropogenic climate change is of societal and scientific interest. Namely, the understanding of extreme melt events, their causes, and future changes in their frequency and intensity are key in developing climate mitigation and adaptation strategies.

Research gap and objectives

The extreme melt event of September 2022 is a recent event with limited research at the time of this research. Previous extreme melt events in Greenland have been studied already extensively. For instance, the extreme melt event of 2012 underwent thorough analysis through the works of Nghiem et al. (2012) and Tedesco et al. (2013), utilizing a range of satellite observations and climate models. Similarly, investigations into the melt event during the summer of 2019, led by researchers like Sasgen et al. (2020), harnessed satellite data to uncover insights. An illustration of an attribution study in the Arctic is the analysis of the high temperature at the North Pole during the winter of 2016 (WWA, 2016). The absence of an attribution study on the September 2022 extreme melt event presents an opportunity to address a knowledge gap in the field.

This study aims to study the influence of human-induced climate change on the September 2022 melt event by means of an attribution study, following adjusted methods of the probabilistic event attribution approach of Philip et al. (2020). This involves understanding the melt event itself, defining its characteristics and investigating the contribution of anthropogenic climate change to the likelihood of the event. Furthermore, this study includes examining the likelihood of similar events occurring in the future.

The main research question in this study is:

"To what extent can the September 2022 Extreme Melt Event at the Summit of Greenland be attributed to anthropogenic climate change and how will the likelihood of such an extreme melt event at the Summit in September change throughout the 21st century?"

The answer to this question will be found with the help of the following sub-questions.

1. How can melt events similar to the September 2022 melt event be detected in observations and model simulations?
2. How rare was the melt event in the current climate based on observations?
3. How has the rarity of the melt event changed over the recent past, based on observations?
4. How much more likely has the melt event become in the current climate, compared to the pre-industrial climate, based on observational data and model simulations?
5. How will the rarity of the melt event change throughout the coming century, based on model simulations of future climate?
6. How much more likely will the melt event become by the end of the 21st century, compared to pre-industrial climate, based on model simulations?

Reading guide

Background information on the September 2022 extreme melt, its causes and the representation of these causes in climate models is provided in chapter 2. An elaborate event definition can be found here as well. In chapter 3 the available data, from observations as well as climate models, is elaborated on. In chapter 4 a description of the methodology is given, encompassing the detection of melt events and the determination of the probabilities and probabilities ratios. In chapter 5 the results can be found, first the thresholds for melt detection are discussed, after which the probabilities and probability ratios resulting from observations as well as climate models are treated. In chapter 6 the results, uncertainties and encounterd issues are discussed. Conclusions and recommendations can be found in chapter 7.

2

Background

In this chapter background information is provided on the extreme melt event in September 2022. The introduction briefly touched upon the event, and within section 2.1, a more extensive elaboration on the event is presented. Subsequently, the causes of the event are discussed in section 2.2. Information on whether these causes can be represented by climate models is elaborated on in section 2.3. Concluding the chapter, section 2.4 offers the event definition, which plays an essential role within the attribution study protocol as formulated by Philip et al. (2020).

2.1. The September 2022 extreme melt event

On the morning of September 2nd, temperatures at the Summit were low but displayed a rapid increase over the course of the day (NSIDC, 2022). The temperature reached a peak in the afternoon of September 3rd when a notable duration of above-freezing temperatures was recorded, with a high of 0.4°C at 15:00 h (NSIDC, 2022). The temperatures remained relatively high on September 4th, slightly surpassing -2°C, and similarly warm conditions prevailed throughout the ice sheet until September 6th. On September 3rd there was a significant rise in air pressure as well, which is commonly associated with melt events at Summit (NSIDC, 2022). The air pressure persisted at elevated levels on September 4th.

During the September melt event, the peak in percentage of ice sheet area showing surface melt, was reached on the 3rd of September. 36% of the ice sheet showed surface melt during that day.

In addition to the extensive melt extent and high temperatures, the amount of meltwater runoff during the September 2022 extreme melt event was also substantial. Typically, the runoff value is below 1 billion tons per day at the beginning of September (Tedesco and Fettweis, 2020). However, during this melt event, the meltwater run-off peaked at nearly 12 billion tons per day on September 3rd, according to data from the Regional Atmosphere Model (MAR) (NSIDC (2022), Tedesco and Fettweis (2020)). This day had the highest run-off total of the whole melting season and ranks among the 10 highest runoff days since 1950 (NSIDC, 2022).

Such a late-season melt event is unprecedented in the satellite era (NSIDC, 2022). Mass balance data covering four decades confirms it was the largest melt event to occur in September so far (Patel and Mooney (2022), Mankoff et al. (2021)). A melt event of this proportion is exceptional to occur this late in the season because the energy coming from solar radiation is already low by then. The most comparable melt event that happened late in the season, occurred in 2003, in late August (NSIDC, 2022). During that event, temperatures rose to -2.5°C at the Summit and a comparable area of the ice sheets' surface experienced melt. In September, melt at the Summit is unprecedented in recent times, however, melt did occur at the Summit in the summer months. Since records started in 1989, surface melt was observed in the summers of 1995, 2012 and 2019 (Moon et al., 2021).

2.2. The causes of the event

The circumstances that led to this late-season melt event were a high-pressure system combined with an atmospheric river (NSIDC, 2022). An atmospheric river is a long, narrow band or corridor in the atmosphere that is responsible for transporting significant amounts of moisture across vast distances. In September 2022, the high-pressure system settled over southern Greenland and drew warm and moist air from the south northward. A low-pressure system to the west of Greenland enhanced the attraction of warm and moist air, by its counterclockwise winds. Due to the clockwise circulation of the winds around the high-pressure system, the warm and moist air arrived at the western edge of Greenland (Lindsey, 2022). The corridor that arose by the winds transporting the warm and moist air, is the atmospheric river.

The warm and moist air flowed from the western side of the ice sheet, where it arrived on September 2nd, over the Summit on September 3rd, towards the southeastern edge on September 4th and 5th (Moon et al., 2022). Together with the warm, moist air came rain at lower altitudes, near the edge of the ice sheet, and snowfall at higher altitudes at the interior of the ice sheet (NSIDC, 2022). The combination of high temperature and humidity values caused the extreme melt event. The rainfall enhanced the surface melt at lower elevations, as well as liquid water clouds enhanced the surface melt over the western edge (Moon et al., 2022).

The large amount of meltwater runoff was a direct consequence of the large melt event in September 2022. A factor that enhanced the high runoff rate, was the rain- and snowfall on the 2nd and 3rd of September. This input of precipitation enhanced the amount of water and snow available for runoff.

Atmospheric rivers (ARs) arrive regularly at Greenland and were not unique for the September 2022 event. A study from Mattingly et al. (2018) showed that atmospheric rivers arrived in higher frequency since the late 1990s. The study showed that from 2000 to 2012, atmospheric rivers played a key role in driving the summertime melt and accumulation. The increased accumulation through snowfall was unable to balance the mass loss through melting, therefore the ARs contributed to the accelerating mass loss of the ice sheet (Mattingly et al., 2018). It is emphasized that the ARs in the highest intensity categories (daily maximum Integrated water Vapor Transport (IVT) more than 85th or 95th percentile) have a much greater impact on the mass balance than ”normal” ARs (daily maximum IVT less than 85th percentile) in terms of melt and accumulation (Mattingly et al., 2018). An example hereof is the 2012 melt event. The intensity of the AR during the September 2022 melt event is not known at the time of writing.

The link between atmospheric conditions and late-season melt events is studied by Ballinger et al. (2019). The results show that the increased water vapour transport by atmospheric rivers is necessary to produce melt events so late in the season. Atmospheric Rivers therefore strongly affect late-season melt events.

2.3. Representation of the causes by climate models

This study requires that the causes of the extreme melt event can be represented by climate models. The aim of this study is to quantify the role of human-induced climate change in the September 2022 extreme melt event. This role can be quantified by comparing the current climate, with anthropogenic emissions, to a counterfactual climate, without anthropogenic emissions. The realization of this counterfactual climate relies upon the simulations by climate models. This comparison is only valuable if events analogous to the September 2022 event can occur in the model simulations. Therefore, it is important to evaluate if climate models are able to simulate both the event and its underlying causes. Specifically, this entails an assessment of the ability of climate models to simulate Atmospheric River characteristics as well as the change of AR characteristics under global warming.

Evaluation of AR simulation

An analysis of the existing literature underscores both advancements and limitations in the ability of climate models to accurately represent ARs and their response to climate change. The findings of Payne and Magnusdottir (2015) highlight the variability in model performance of GCMs from Coupled Model Intercomparison Project Phase 5 (CMIP5) over the North Pacific. CMIP5 is an international research effort conducted by numerous climate modelling groups aimed at improving our understanding of the Earth’s climate system and its future projections. Most models are capable of capturing the

spatial structure of AR-landfalling events, yet they are struggling to reproduce frequency distributions and interannual variability. Ramos et al. (2016) and Lavers et al. (2013) extend these investigations to European ARs, affirming the ability of CMIP5 models to simulate AR-like patterns, albeit with biases and uncertainties. Kim et al. (2023), focusing on CMIP6 models over East Asia, acknowledge biases while indicating potential in representing AR characteristics. The models tend to underestimate the magnitude of the spatial variability of the AR properties. Zhao (2020) insights into the capabilities of CMIP6 models for AR characteristics offer promise, although regional biases persist.

The performance of climate models simulating AR over Greenland has not been researched extensively. Neff (2018) studied the role of AR in controlling mass loss of the Greenland ice sheet. They state that climate models do not predict robust changes in the North Atlantic Oscillation (NAO) and thereby prevent reliable projections of AR-related melt on Greenland. No further research specifically for Greenland has been found.

Necessity of high spatial resolution

The spatial resolution of climate models plays an important role in accurately capturing AR features, as emphasized by Huang et al. (2020), Guan and Waliser (2017) and Liu et al. (2022). A 40-60% improvement is found for simulation with a 3 km spatial resolution compared to simulations with a 27 km spatial resolution by Huang et al. (2020). Guan and Waliser (2017) and Liu et al. (2022) endorse these conclusions, however, consistently large errors were found for 7/17 AR characteristics. Liu et al. (2022) compare simulated ARs in high-resolution (HR) and low-resolution (LR) CESM simulations against observations. They conclude that the strength and associated precipitation of ARs are severely underestimated and that the response to major climate modes is poorly simulated in the LR CESM simulations. However, the seasonal shifts of ARs' occurrence frequency can be well simulated. The HR CESM simulations show substantial improvements in simulating AR characteristics and statistics. The relationship with major modes of climate variability is improved for HR in comparison with LR, as well as the simulated precipitation over landfalling regions.

Evaluation of the response to Global Warming

The response of ARs to a warming climate is an important aspect and can be captured reasonably well by GCMs in specific regions, such as the North Pacific (Payne and Magnusdottir, 2015) and Europe (Ramos et al., 2016), as well as for the whole Earth (Espinoza et al. (2018), Zhang et al. (2021), Kay et al. (2015)). An increase in AR frequency, an increase in AR moisture transport and an increase in the number of ARs at the end of the century are projected by most models. Espinoza et al. (2018) validates the multi-model mean of historical simulations against ERA-Interim data and they conclude that the historical multi-model mean is a good representation of the observations, with a small low bias.

Limitations and implications

From the above, it becomes clear that, while progress has been made in simulating ARs and their response to climate change, critical limitations persist. Climate models have made strides in representing ARs, particularly models with a high resolution showed improved results. However, large uncertainties and local biases persist in the models and the region of Greenland is barely researched. This poses limitations and does not provide convincing evidence that large and rare AR can be accurately simulated in Greenland. The limitations underline the need for recognizing the constraints when using climate models for this attribution study and prudence in interpreting the results. In conclusion, while the existing literature falls short of providing convincing evidence for the representation of the extreme event's causes within climate models, this attribution study employs climate models while carefully considering their inherent limitations.

2.4. The event definition

The probabilistic event attribution analysis asks for a clear event definition that relates closely to the rarity of the event. Here, the role of human-induced climate change on the likelihood of 'melt at the Summit' is investigated. The September 2022 melt event was extreme in its high melt extent, high runoff rate and high temperatures resulting in melt at the Summit and all of this occurring late in the season, in September. All three metrics are worth studying, however, ´melt at the Summit´ is selected as the metric under study, because it relates closely to the rarity of the event; Melt at the Summit

is unprecedented for September in the satellite era and occurs scarcely in other months of the year. The exceptionality of melt at the Summit also comes with a downside, namely the lack of data points available as input for this study. Therefore the analysis plan is extended to take both September as well as all other months into account for the analysis.

The likelihood of melt at the Summit is defined as the likelihood of 'a year with melt'. When one hour, day or month shows a sign of melt above the set threshold, the year is registered as a year with melt.

In summary, the attribution question has been specified as:

"How has the likelihood of a year with melt at the Summit in Greenland, in September as well as in all months, changed due to anthropogenic emissions?"

Melt at the Summit in Greenland is available as a variable in several observations as well as in climate models, which is necessary data for the attribution study to be feasible. More information on the data can be found in chapter 3.

3

Data

This chapter provides an overview of the Area of Interest (AOI) and the observational and climate model data utilized in this research. This research demands a long time span of historical observations, in order to determine the probability of an extreme melt event in the current climate as well as in the past, pre-industrial climate. This research demands climate model data in order to determine the probability of an extreme melt event in a future climate, the pre-industrial climate and the current climate. The specific types of observational data employed in this study comprise ice core data (section 3.3), station data (section 3.4), passive microwave satellite data (section 3.5), reanalysis forced RACMO data (section 3.6.1) and reanalysis forced MAR data (section 3.6.2). The climate model data employed in this study comprises CESM HR data (section 3.7).

3.1. The Summit; area of interest

The designated area of interest for this study is a circular region with a radius of 45 km around the top of the Greenland ice sheet. This circular boundary encompasses most land areas situated at or above the altitude of Summit Station (3210 m), see figure 3.1. By considering an area that encompasses most land above 3210 m, the study aims to account for all potential instances of melting at such elevations. Hereby the AOI includes the highest point of the ice sheet, as well as the highest point where in-situ measurements are available, providing valuable data for analysis. The circular shape is chosen for practical reasons, facilitating ease of processing. All data points falling within this defined area of interest will be included when studying melt at the Summit. Figure 3.1a illustrates the geographical location of the AOI within Greenland, figure 3.1b illustrates a height map of the area around the Summit of Greenland with the AOI and Summit Station indicated. The latitude-longitude coordinates of the centre of the AOI are [72.5319 $^{\circ}$N, 37.7185 $^{\circ}$W], the radius is 45 km and the area is 6362 km^2.

3.2. Time periods of interest

This study requires the delineation of three distinct time periods to examine the pre-industrial climate, the current climate, and the future climate in observations and climate model data. For both the current en future climate, a time span of 30 years is selected. This time span is a compromise between two factors: the need for a sufficiently long duration to establish a representative mean of the data, and the desire for a relatively short duration to ensure a stable climate without large changes. Consequently, a period of 30 years is chosen as it provides a representative snapshot of a consistent climate over that time frame.

For the representation of the current climate, the time range from 1990 to 2020 is selected. This definition intentionally omits the event that triggered the analysis. This decision serves two purposes: first, to mitigate potential bias in the probabilities towards the extreme (Philip et al., 2020), and second, to align with the data availability, which typically extends only up to 2021 rather than encompassing the entirety of 2022. These reasons substantiate the decision to analyse the period from 1990 to 2020 and omit the September 2022 event.

To project the future climate, the period spanning from 2070 to 2100 is chosen. This particular time

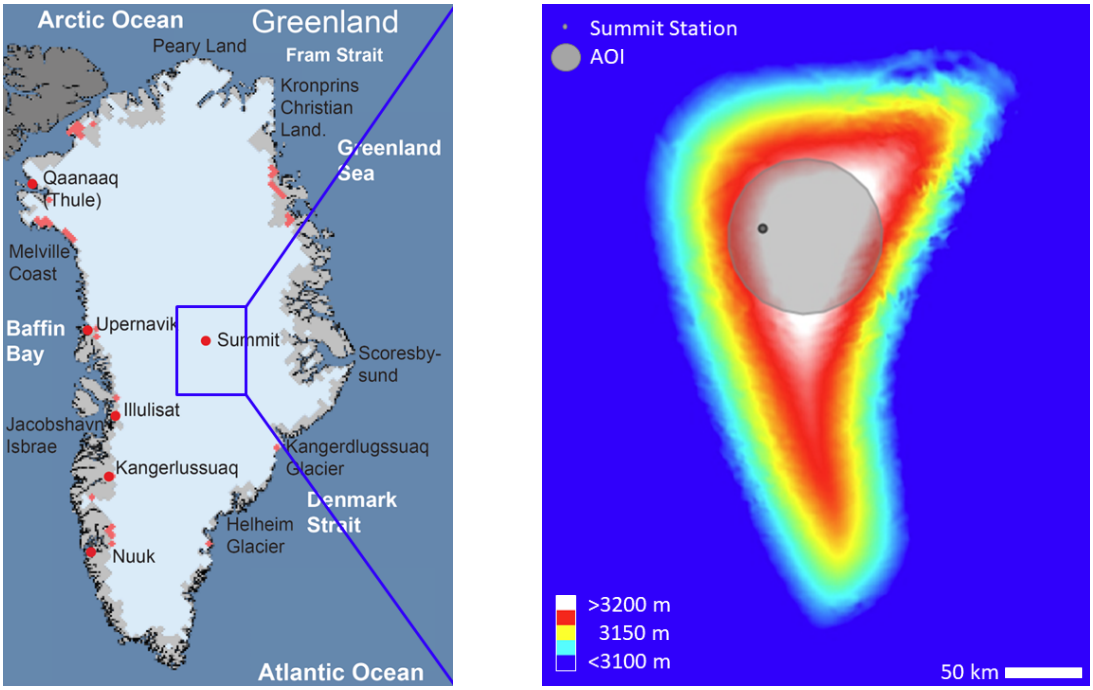

(a) Map of Greenland indicating AWS stations, including Summit Station. Outline of height map in blue.

(b) Height map of the centre of Greenland, with Summit Station (height=3210m) and the AOI indicated

Figure 3.1: Greenland and the Area Of Interest

frame strikes a balance, being the furthest projection into the future while still falling within the range of available climate model data.

The definition of the pre-industrial period exhibits a degree of flexibility compared to the other two defined periods. This era is characterized by the minimal influence of human-induced emissions on the climate state. Given that until the commencement of the 19th century, anthropogenic emissions had a limited impact on the climate, timeframes dating back to 1900 and earlier are considered within the scope of the pre-industrial period. In instances where observations of the pre-industrial period encompass years beyond 1900, a judicious assessment is undertaken to determine whether the data should be considered or not. Within the climate model data, the pre-industrial period is represented by the year 1850.

3.3. Ice core data

A valuable source of in-situ data at the Greenland ice sheet is ice core data. Ice core data can help reconstruct past climate conditions up to 800,000 years ago (Alley, 2000) and provide additional context to station data, satellite observations and reanalysis data. An ice core is a vertical column of firn and ice that is removed from the ice sheet by drilling. An ice core is a sample of the layers of snow that formed through yearly snowfall and snow melt. The layers of snow turned into ice under high pressure and contain a record of past climate conditions, including temperature, atmospheric composition, volcanic eruptions and human activity. The presence of melt can be determined with a temporal resolution of one year.

On the Greenland Ice Sheet, ice cores are drilled in several locations, including at the Summit. Two studies (Alley and Anandakrishnan (1995), Meese et al. (1994)) are done on the GISP2 (Greenland Ice Sheet Project 2) ice core, which was bored at the Summit, that focus on the Holocene period, spanning from 10,000 years ago till present. Three other studies (Keegan et al. (2014), Trusel et al. (2018), Clausen et al. (1988)) focus on a shorter time span: the last 350 years. They study ice cores bored at the Summit as well as at other locations spread across the ice sheet. An overview of all ice core data sources, the period they cover and their locations, can be found in table 3.1.

Ice Core Data Source	Length	Period	Sites
Keegan et al. (2014)	250 years	1750-2012	Summit-2007, Summit-2010, D4, ACT 3, NEEM 2008 S1, NEEM 2009 S2
Trusel et al. (2018)	350 years	1650-2015	Central West Greenland (D5+GW+GC)
Clausen et al. (1988)	360 years	1622 - 1984	A-H (Summit)
Alley and Anandakrishnan (1995)	10.000 years	8.000 BC - 1993	GISP2 (Summit)
Meese et al. (1994)	11.000 years	9.000 BC - 1993	GISP2 (Summit)

Table 3.1: Ice Core data overview

3.4. Station data

Greenland is a large, sparsely populated country and has little in-situ observations. However, a network of Automatic Weather Stations (AWS) is operated by the Greenland Climate Network (GC-Net) and counts just over forty stations distributed over Greenland. The first station was operative since 1991 and the network has expanded ever since (Steffen et al., 2020). Since May 1996 a GC-Net station near the Summit of Greenland has been operational. 'Summit Station' is located at an elevation of 3210 m at latitude-longitude coordinates [72.5797 °N, 38.5045 °W] near the Summit of the Greenland ice sheet (NSF, Summit Station Science Coordination Office, 2023).

The GC-Net station records several variables, including air temperature, humidity, wind speed and direction, incoming and reflected shortwave radiation and air pressure. All variables are measured hourly and the data is transmitted in near-real time on most occasions. For this study, Level-1 data is utilized. Level-1 data is pre-processed and available in CSV-compatible NEAD format (Steffen et al., 2020). From the available variables, the variables used in this study are air temperatures TA1 and TA2 and specific humidities Q1 and Q2. These variables are measured at 2 varying heights above the surface approximately 1 meter apart, the details of this station are described by Vandecrux et al. (2023). Therefore the average of each pair of variables is taken and used for the analysis. These new variables are referred to as TA (the mean of TA1 and TA2) and Q (the mean of Q1 and Q2) in the remainder of this study.

A second source of station data utilized in this study is the Greenland Environmental Observatory (GEOSummit). This facility was established by the U.S. National Science Foundation (NSF) and the Danish Commission for Scientific Research in Greenland to provide year-round, long-term measurements for monitoring and investigations of the Arctic environment (NSF, National Science Foundation Office of Polar Programs, 2023). The observatory at the Summit is located at latitude-longitude coordinates [72.5962 °N, 38.4220 °W] and performed meteorological measurements between 25 June 2008 and present. Data is available for the period 25-06-2008 until 30-07-2022 in hourly and minute resolution. The hourly data has a sufficient temporal resolution for this research and can be easily compared to the other station data, therefore this resolution, and not a higher resolution, is used. Three temperature variables are available: temperature at 2 meter height, at 10 meter height and at the tower top. The 2m air temperature ($TA2m$) is used in this study, as well as the Relative humidity (RH).

Instrument	Location	Time period	Variables	Resolution
GC-Net AWS	Summit station	13-05-1996-	TA (Air temperature)	Hourly
		07-10-2022	Q (Specific humidity)	Hourly
GEOSummit AWS	Summit station	25-06-2008-	TA2m (Air temperature)	Hourly
		30-07-2022	RH (Relative humidity)	Hourly

Table 3.2: Overview station data

3.5. Satellite Passive Microwave data

Next to in-situ observations, satellite observations are a valuable source of data for Greenland. A satellite data source used for observing melt is Passive Microwave data (Picard (2022), Picard (2023)).

Passive Microwave data provides a melt/no-melt value for every pixel over Greenland. The snow melt value is derived using the method developed by Picard and Fily (2006). This method encompasses taking the daily mean of all radiometer measurements whose footprint centre falls into a pixel during 24h. To the daily mean brightness temperatures, an adaptive threshold is applied to determine melt/no melt.

This study uses a fully processed dataset that provides daily surface melting data derived from SMMR and SSM/I Passive Microwave data (Picard, 2022). This "Daily Surface Melting Dataset" has a spatial resolution of 25 x 25 km and covers the land area of Greenland. The dataset has a temporal resolution of 1 day (2 days before 1988), and its temporal coverage ranges from 1-11-1979 to 5-1-2022. For data more recent than January 2022, a NRT dataset is available.

The NRT dataset, provided by Picard (2023), has snowmelt derived from the AMSR2 Passive Microwave data. This dataset has a spatial resolution of 12.5 x 12.5 km, twice as high as the fully processed dataset, and covers the same area. The dataset has a temporal resolution of 1 day, and its coverage ranges from 05-04-2022 to 01-11-2022. The NRT dataset thereby complements the fully processed dataset. It should be noted that the near-real-time processing is subject to various types of errors, and the observations should be interpreted with care (Picard, 2023).

To prepare the data for analysis, the data points located within the Area of Interest (AOI) are selected. For the fully processed data, this yields nine data points. The selected data points are visually represented in figure 3.2, along with all other data points of the dataset.

PM data version	Sensor	Temporal resolution	Temporal coverage	Spatial resolution	Grid
Fully processed	SMMR, SSM/I	Daily	1-11-1979-5-1-2022	25x25 km	Stereographic polar grid
NRT	AMSR2	Daily	05-04-2022-01-11-2022	12.5x12.5 km	Stereographic polar grid

Table 3.3: Passive Microwave (PM) data overview: fully processed and Near Real Time (NRT)

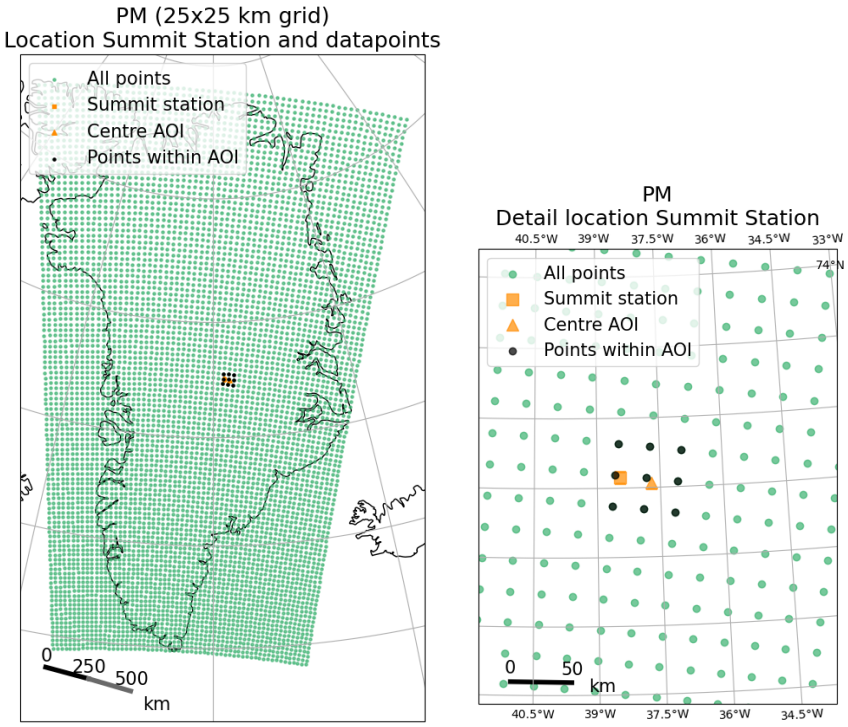

(a) Overview Greenland

(b) Detail data points within AOI

Figure 3.2: Location Summit station and data points over Greenland (25x25 km grid) (map crs = Stereographic)

3.6. Reanalysis forced RCM data

Another data source is the output from the Regional Climate Model (RCM) forced by Reanalysis data. Reanalysis involves combining models with observations to create comprehensive global datasets that depict the recent historical climate (ECMWF, 2023). It provides estimates of atmospheric and surface parameters for all locations on Earth, spanning several decades. Regional climate models use the reanalysis data to force the conditions at its lateral boundaries and sea surface. By employing reanalysis data for forcing, the RCM can accurately reproduce the climate as it truly transpired, closely mimicking the timing of events. The RCMs are capable of simulating climate conditions at high spatial and temporal resolutions, offering advantages over relying solely on reanalysis data. The Reanalysis forced Regional Climate Model data is used to analyse the current climate and the recent past and complements the in-situ and satellite observations. Two specific regional climate models designed for the polar regions, and used in this study, are the Regional Atmospheric Climate MOdel (RACMO) and the Modèle Atmosphérique Régional (MAR).

3.6.1. ERA forced RACMO

The Regional Atmospheric Climate Model (RACMO) is a regional climate model initially developed by the KNMI (Royal Netherlands Meteorological Institute) and the DMI (Danish Meteorological Institute) in 1990 (IMAU, Institute for Marine and Atmospheric Research, 2023). It is based on the High-Resolution Limited Area Model (HIRLAM) numerical weather prediction model. RACMO2, the second version of RACMO, integrates the dynamical core of the HIRLAM model with the European Centre for Medium-range Weather Forecasts (ECMWF) Integrated Forecast System (ISF) physics to improve the representation of extreme conditions over ice sheets and glaciers.

Due to its regional nature, RACMO requires external information to force its lateral boundaries and sea surface. The model's top is left unforced, and the interior of the model is not nudged towards observations, allowing it to evolve freely. RACMO2 provides a realistic simulation of surface mass balance (SMB) and exhibits good agreement with observations, owing to its detailed snow scheme (Rae et al., 2012). Moreover, the model accurately reproduces the observed trend of increasing melt area in recent years, as inferred from satellite measurements of microwave brightness temperature (Rae et al., 2012).

For this study, output from RACMO version 2.3p2 is utilized. The inclusion of 'p2' in the version number indicates that this particular iteration of RACMO has been specifically modified for polar conditions (IMAU, Institute for Marine and Atmospheric Research, 2023). According to a study conducted by Noël et al. (2018), RACMO2.3p2 demonstrates good performance in simulating the climate of the Greenland ice sheet. The data has a spatial resolution of 1x1 km on a Polar Stereographic North-grid, which is statistically downscaled from the 5.5x5.5 km resolution output of RACMO2.3p2. The data encompasses the period from January 1958 to December 2021 with a daily resolution. To force the Regional Climate Model (RCM), three generations of ERA reanalysis data are employed: ERA-40, ERA-Interim, and ERA5 for the periods 1958-1978, 1978-1989, and 1990-2021, respectively. The ERA reanalysis datasets are a reanalysis product provided by the European Centre for Medium-Range Weather Forecasts (ECMWF).

The variable used for this study is "Downscaled corrected snowmelt," expressed in millimetres water equivalent per day ($snowmeltcorr\ [mm\ w.e.\ per\ day]$).

A total of 6314 selected pixels fall within the AOI, each with an area of 1 km2. See figure 3.3 for the location of the pixels within Greenland and the AOI.

RACMO data version	Forced by	Temporal coverage	Temporal res.	Projection	Spatial res.
2.3p2	ERA-40 (1958-1978) ERA-I (1979-1989) ERA5 (1990-2021)	01-01-1958- 31-12-2021	Daily	Polar Stereographic North	1x1 km2

Table 3.4: RACMO data overview

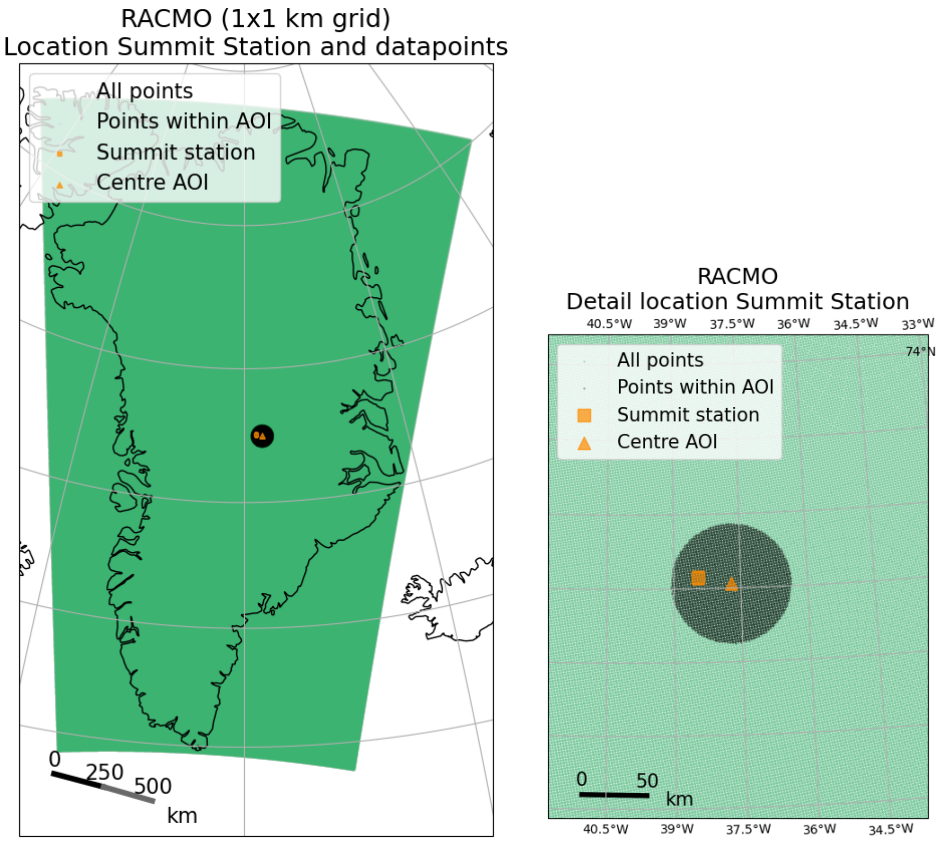

(a) Overview Greenland

(b) Detail data points within AOI

Figure 3.3: Location Summit station and data points over Greenland (1x1 km grid) (map crs = Stereographic)

3.6.2. ERA forced MAR

The Modèle Atmosphérique Régional (MAR) is a regional climate model developed by the University of Liège to study the polar regions. MAR is forced by ERA5 reanalysis data and coupled to the Soil Ice Snow Vegetation Atmosphere Transfer Scheme (SISVAT), a vegetation-atmosphere model that models the first 30 m of snow and the first 10 m of soil in multiple layers (Mankoff et al., 2021). The snow model is based on the CROCUS snow model, which deals with all snowpack processes.

MAR gives a realistic simulation of SMB (Rae et al., 2012). It agrees well with observations because the model has a detailed snow scheme. The trend of increasing melt area in recent years, inferred from satellite measurements of microwave brightness temperature, is well reproduced by the model (Rae et al., 2012).

The model output used for this study is the version 3.12.1 daily output with a spatial resolution of 10x10 km on a polar stereographic grid. The temporal period that is covered is from January 1950 to December 2021. The available variables of interest in the daily data are Meltwater production ($ME\ [mmWE/day]$), Temperature ($TT\ [°C]$) and Specific Humidity ($QQ\ [g/kg]$).

A total of 64 pixels fall within the Area Of Interest, each with an area of 100 km2. See figure 3.4 for a detailed view of the pixels within Greenland and relative to the Summit and Summit Station.

MAR data version	Forced by	Temporal coverage	Temporal res.	Projection	Spatial res.
v3.12.1	ERA5	01-01-1950-31-12-2021	Daily	Polar Stereographic	10x10 km2

Table 3.5: MAR data overview

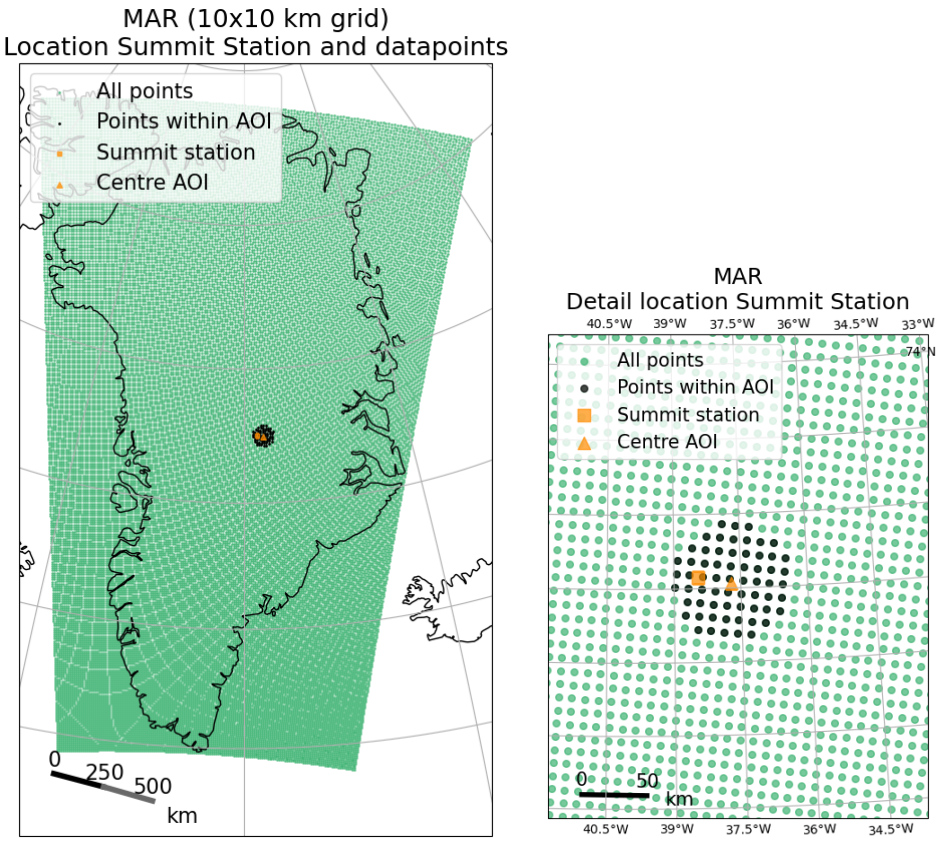

(a) Overview Greenland

(b) Detail data points within AOI

Figure 3.4: Location Summit station and data points over Greenland (10x10 km grid) (map crs = Stereographic)

3.7. Community Earth System Model High Resolution data

The climate model data used in this study are the CESM HR simulations. The Community Earth System Model (CESM) is a fully coupled global climate model that provides state-of-the-art computer simulations of Earth's past, present and future climate states (NCAR, 2023). It is developed by the National Centre for Atmospheric Research (NCAR) in collaboration with the broader climate modelling community to understand climate variability and global change.

The international Laboratory for High-Resolution Earth System Prediction (iHESP) used the CESM to generate global climate datasets in high-resolution (CESM HR). The CESM HR datasets are generated using a high-resolution configuration of the Community Earth System Model version 1.3 (CESM1.3) (iHESP, 2023). The CESM version 1.3 is used for the HR runs, and not the more recent CESM version 2, because there was no high-resolution configuration available yet for this version. Also v1.3 is thoroughly evaluated for simulations with a high-resolution configuration (Small et al., 2014).

The atmosphere and land models have a nominal resolution of 0.25 degrees and the ocean and sea-ice models have a nominal resolution of 0.1 degrees. This allows for interactions between synoptic and mesoscale phenomena with large-scale circulations, which is of importance for Atmospheric River modelling.

Model	Version	Grid	Temporal resolution	Component	Spatial resolution
CESM	1.3	ne120np4_tx0.1v2 (HR)	Monthly	*CLM4.0*	*0.25°*
				CAM5.4	0.25°
				POP2	0.1°
				CICE4.0	0.1°

Table 3.6: CESM Atmosphere, Ocean, Land, Sea-ice and River-transport coupled model

The CESM HR collection has several types of runs that are of interest, namely the pre-industrial control simulations and the transient simulations. The transient simulations were branched from year 250 of the control simulation. It uses historical forcings from 1850 to 2005 and representative concentration pathway 8.5 (RCP8.5) forcings from 2006 to 2100 in accordance with CMIP5 experimental protocol. RCPP8.5 is the most extreme future scenario, where greenhouse gas emissions are high.

The simulations are indicated with the names ”Historical run”, referring to the historical part of the transient simulation, ”Future run”, referring to the RCP8.5 part of the transient simulation and ”Control run”, referring to the pre-industrial control simulation. The pre-industrial control run has 500 years of simulation and the transient simulation has 250 years of simulation. For the transient simulation, three ensembles/runs are available. For an overview of this information, see table 3.7.

Name (abb.)	**Simulation**	**Timespan per ensemble**		
		E1	**E2**	**E3**
Historical (HIST)	1850 Transient simulation (Historical)	1850-2005	1920-2005	1920-2002
Future (FUT)	1850 Transient simulation (RCP8.5)	2006-2100	2006-2100	2006-2100
Control (CTRL)	1850 Pre-Industrial Control simulation	500yr	-	-

Table 3.7: CESM HR available runs

From this model and these runs, three variables are of interest: Melt, Temperature en Humidity. The choice for which specific variables are used is elaborated on below. All three variables are part of the ’land’ part of the CESM model, the Community Land Model 4.0, and have a spatial resolution of 0.25°.

The main variable of interest is melt. The Community Land Model from the CESM outputs various variables related to melt. Most variables are related to the heat flux generated by snow melt, one variable is a measure that quantifies the melt in mm/s: $QSNOMELT\ [mm/s]$. This variable can represent the total melt at the summit well.

The second variable of interest is temperature. The temperature variable is needed for the detection of circumstances that indicate the presence of an atmospheric river. For the detection of atmospheric rivers, the air temperature is a suitable temperature to use. In the CESM data, multiple temperature variables are available. The 2m Air Temperature will be used in this study: $TSA\ [K]$. The temperature values in the CESM output are stored in Kelvin. For this study, the temperature values are converted to Celsius via the formula $TSA\ [°C] = TSA\ [K] - 273.15$.

The third variable, also needed for AR detection, is humidity. There are two main options for humidity. The specific humidity and the relative humidity. The specific humidity is used by other studies to determine the Integrated Water Vapor Transport (IVT), which is then combined with vector winds to detect atmospheric rivers (Guan and Waliser (2017), Payne and Magnusdottir (2015)). Therefore the specific humidity will be used in this study as well. In the CESM data, the Specific Humidity is defined as: $Q2M\ [kg/kg]$.

The CESMHR dataset covers all land parts of the globe with a 0.25° x 0.25° grid. For the scope of this research, only the data points in the Area of Interest (AOI) are of interest. The eight data points within the AOI as well as all other data points around Greenland are visualised in figure 3.5.

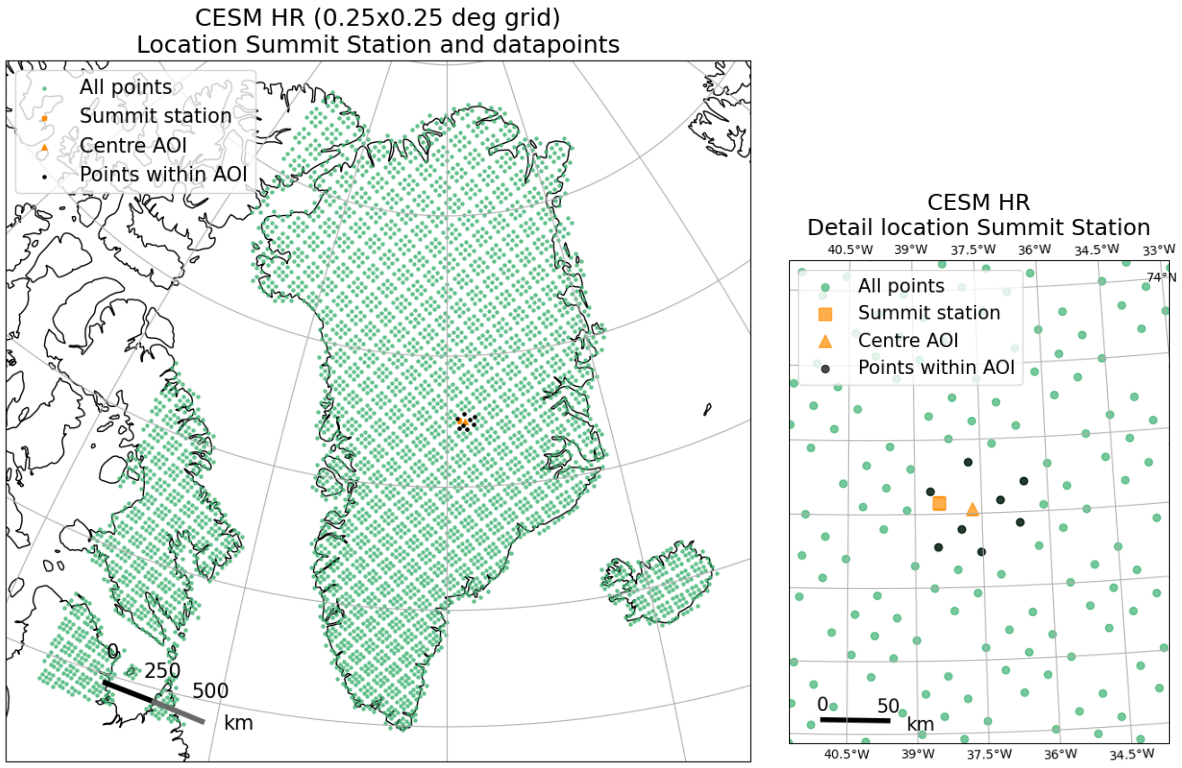

(a) Overview Greenland

(b) Detail four closest data points

Figure 3.5: Location Summit station and data points over Greenland (0.25x0.25 deg grid) (map crs = Stereographic)

4

Methodology

The aim of this chapter is to provide a detailed overview of the approaches and techniques used to analyze the data and derive meaningful insights. This chapter introduces first the general approach employed in this study to investigate the research questions outlined in chapter 1. Furthermore, the specific methods that are employed are elucidated. The process of detecting melt events and establishing thresholds for melt detection and AR detection are discussed in section 4.1. Section 4.2 focuses on the computation of probabilities and probability ratios to assess the occurrence of melt events. Finally, section 4.3 explores the analysis and synthesis. By delineating these methods, this chapter sets the foundation for the subsequent analysis and discussion presented in the following chapters.

The general approach can be summarized in the following steps:

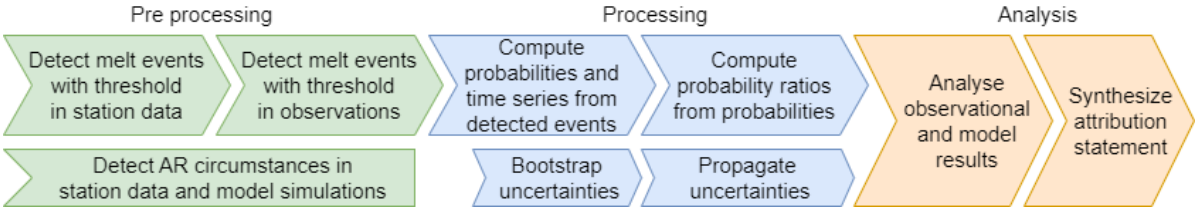

Figure 4.1: General approach of the method applied in this study

4.1. Detection of melt events caused by Atmospheric Rivers

In order to compute the probability of extreme melt events caused by AR, it is important to first detect the events in the data. The detection of events is done by setting a threshold on the melt, temperature and humidity variables. Since the format of the variables varies across different data sources, a distinct threshold is established for each source. Nevertheless, the objective is to ensure that the thresholds remain as consistent as possible. The detection of melt and the detection of Atmospheric River circumstances is elaborated on below.

4.1.1. Detection of melt

In station data

The detection of melt events from the Station Data follows a different method than the detection of melt events in spatial data. The Summit Station data encompasses no melt variable, this variable is not measured nor computed from the given variables. Melt can be computed by solving the energy balance, however, the computation of melt with the energy balance from the station data is hard, due to missing variables. Therefore the temperature is used as a proxy variable to determine 'melt' events. The events that are detected, are events with a temperature at Summit Station above 0 degrees Celsius.

For the GC-Net station data, the mean temperature at the station and the 2m air temperature are options for the proxy variable. The mean temperature at the station (TA) is used, because this variable

has fewer data gaps than the 2m air temperature ($TA2m$). The accuracy of the instrument is 0.1°C, therefore a threshold of 0 - 0.1°C is used.

$$TA >= -0.1°C$$

The results are screened for non-physical values. All temperature readings above 5°C are not realistic at Summit station and therefore discarded, following Hanna et al. (2014). Also, all above-zero temperature readings in January, February, March, October, November and December are deemed erroneous and are therefore discarded. After a visual check, two more events were deemed erroneous due to one of the values of $TA1$ or $TA2$ being far above 5°C.

For the GEOSummit Station Data, the 2m air temperature, 10m air temperature and the temperature at the tower top are the options for the proxy variable. The 2m air temperature ($TA2m$) is the most convenient temperature to use since it is closest to the surface. Therefore it is the chosen variable for this station. The accuracy of the instrument is 0.1°C as well, therefore the threshold for a temperature-above-zero-event is set to -0.1°C.

$$TA2m >= -0.1°C$$

The resulting events were screened for non-physical values by visual inspection, no erroneous readings were found.

In spatial data

In order to detect melt events in the spatial data, it is necessary to establish a threshold for the *number of data points* indicating a melt event and to establish a threshold for the *amount of melt per pixel* indicating melt.

The threshold for the number of data points indicating melt within the AOI is based on the exceptionality of the event. The AOI encompasses all regions at or above the altitude of the Summit station. The presence of melt within this AOI is considered exceptional. Therefore, if even a small portion of the AOI exhibits signs of melt, a melt event is identified. This "small part" is defined as approximately $\frac{1}{10}$ of the AOI, which corresponds to an area of 636 km^2. This specific area is selected because it is similar in size to the pixels found in the datasets with the coarsest resolution. Specifically, the PM dataset contains pixels with an area of 625 km^2 and the CESM HR data has pixels of approximately 461 km^2 or 1156 km^2, due to its grid. If an x amount of pixels, together approximating an area of 636 km^2, shows melt, a melt event is detected.

When the thresholds for a melt event are determined, the thresholds for melt at single data points are determined per data source. A pixel shows melt if the value is more than or equal to the threshold value x. The threshold per pixel has a big influence on the amount of melt events that are detected and thus on the resulting probability. Therefore a well-considered choice is made on which threshold to use.

The Passive Microwave data around the Summit consists of nine pixels. Their snowmelt value is derived from the brightness temperature and is either 0 (indicating no melt) or 1 (indicating melt). Per data point it is clear if melt is detected or not, therefore no further threshold needs to be set for the Passive Microwave data. The Passive Microwave melt data is screened for non-physical values by visual inspection, thereby one melt event in December was found to be erroneous.

To determine the threshold for both RCM datasets, the best agreement is sought between melt events in the RCM data and events with temperatures above zero in the Summit station data. The Summit station data is used as the reference data because this encompasses direct observations with a high, hourly resolution. The thresholds that are taken into account for this analysis are chosen based on literature.

The method applied to find the melt threshold for the RCM data, cannot be applied to find the threshold for the CESM HR data. The CESM HR data is a global climate model that is forced by the statistics of past climate, but not by the exact climate as it happened in time. Since the CESM HR data is not a reconstruction of the past, melt events will not necessarily appear in the exact same years, months or days. Therefore, no direct comparison with the station data can be made. However, melt events are assumed to appear with the same frequency in the climate model simulation as in the past. Therefore, the best agreement is sought between the probability of events with temperatures above zero in the Summit Station data and the probability of melt events in the CESM HR simulations. CESM

HR dataset consists of three ensembles, E1, E2 and E3. All three ensembles are inspected in order to find the best agreement with the Summit Station data.

Furthermore, a melt event is defined as the occurrence of at least one day with melt. If there are multiple consecutive days with melt, they are counted as a single event. However, if days with melt are interspersed with at least 5 days without melt in between, they are considered separate melt events.

4.1.2. Detection of Atmospheric River circumstances

Detecting Atmospheric River (AR) circumstances plays a pivotal role in contextualizing melt events within the scope of this study. The identification of AR conditions relies on examining temperature and humidity, which serve as key indicators of AR presence. Subsequently, a specific threshold is established for these variables. It is noteworthy that the process of detecting atmospheric rivers is intricate and cannot be simplistically replaced by merely considering temperature and humidity parameters. Thus, this study does not aim to directly detect atmospheric rivers but instead focuses on observing whether similar conditions to those observed during the September 2022 AR melt event occurred, indicating the potential presence of AR. From the data sources included in this study, the temperature and humidity variables are obtainable from Station data, MAR data, and CESM HR data. For the observational period, the Station data is chosen to be analyzed due to its superior temporal resolution. For the climate model data, the only option is to use the climate model data itself.

In Station data

AR circumstances are identified within the GC-Net station data to provide context for the melt events detected in historical observational data. Within the Station data, a day is classified as having AR circumstances if it satisfies either of the following two criteria:

1. The daily maximum temperature and daily maximum humidity exceed the corresponding daily maximum values recorded on the day of the extreme melt event, September 3, 2022.
2. The daily mean temperature and daily mean humidity surpass the respective daily mean values of September 3, 2022.

To address measurement uncertainties, as provided by Vandecrux et al. (2023), a threshold adjustment of 0.1°C for temperature and 10% for humidity is applied. This adjustment ensures that AR events are not overlooked during the detection process.

In Climate model simulations

AR circumstances are identified within the climate model simulations to provide context for the melt events detected within those simulations.

Given that the CESM HR model operates with a monthly temporal resolution, the threshold for identifying AR circumstances is derived from the monthly mean temperature and monthly mean humidity recorded in the Station data for September 2022. A month within the CESM HR data is classified as potentially having experienced an AR event if it satisfies the following criterion:

1. The monthly mean temperature and monthly mean humidity exceed the corresponding monthly mean values recorded by the GC-Net station in September 2022.

It's important to emphasize that AR events typically occur on an hourly to daily scale, a level of detail not captured by the monthly resolution of the climate model data. Consequently, this method does not claim to directly detect AR events themselves but rather highlights instances where an AR event could have influenced the monthly mean, as it resembles the monthly mean values of the extreme event in September 2022.

In September 2022, the mean temperature increased by 1.72°C (from -16.71°C to -14.98°C) due to the melt event and the mean specific humidity increased by 0.31 g/kg (from 1.56 g/kg to 1.87 g/kg) according to measurements at Summit station (see Appendix A, figure A.1 and A.2). This is a phenomenon that could potentially be replicated in the model simulations. However, the extent to which an extreme event affects the mean is contingent upon the baseline mean temperature. In cases like summer months, when the mean temperature is already elevated, an extreme event may exert a less significant impact on the mean. Thus, monthly mean temperatures and humidities exceeding those of the September 2022 event may suggest the occurrence of an AR event but do not definitively confirm it.

While it's acknowledged that this method may not achieve the desired level of robustness, it nonetheless represents the most practical approach within the constraints of the available data.

4.2. Probabilities and Probability Ratios

After event detection, the subsequent phase involves the computation of probabilities pertaining to melt events caused by atmospheric rivers. Due to data limitations, a simple method is employed to estimate these probabilities. The extreme nature of these events results in the vast majority of values being zero, with only a few exceeding zero. Consequently, it is not feasible to fit a distribution to the data for the purpose of computing probabilities. Instead, these probabilities are determined empirically.

Probabilities

The probabilities that are defined are the probability of "a year with melt" (p_{All}) and the probability of "a year with melt in September" (p_{Sep}). If multiple melt events happen in one year, the probability of "a year with melt" is not affected. The probability can be empirically computed by dividing the number of years with at least one melt event by the total number of years. The return time (T_{All} or T_{Sep}) of a melt event can be computed by dividing 1 by the probability. In other words, by dividing the total number of years by the number of years with at least one melt event.

Probability time series

Probabilities and return times in this study are calculated based on a period of 30 years, as defined in section 3.2. A time series of probabilities is constructed by computing the probabilities for multiple consecutive and overlapping periods. The probability over 30 years is computed with increments of 1 year for the available time spans. The value of a period of 30 years is allocated to the centre year of the period. E.g. for a time series with data between 1960-1992, the probabilities are computed for 1960-1990, 1961-1991 and 1962-1992 allocated to the years 1975, 1976 and 1977 respectively.

Probability Ratios

When the probabilities are known, they can be used to compute the probability ratio between various climates (and time periods). The probability ratio is an expression of the change in frequency of extreme melt events due to anthropogenic climate change. The Probability ratio (PR) is the ratio between the probabilities of an event occurring in two distinct climates. E.g. it is the probability of the extreme event occurring in the current climate (p_1) divided by the probability of the extreme event occurring in a counterfactual climate (p_0) without anthropogenic emissions $PR = \frac{p_1}{p_0}$ (Philip et al., 2020).

A counterfactual climate is a climate that could have existed but does not exist. A counterfactual climate without anthropogenic emissions therefore is a simulation of how the climate would have looked like, if there had been no emissions of greenhouse gasses by humanity. For this study, the pre-industrial climate is taken as the 'counterfactual climate', the climate without anthropogenic emissions.

The probability ratio can also be computed for the future climate. In that case, p_1 is the probability of the extreme event occurring in the future climate and p_0 is the probability of the extreme event occurring in the counterfactual climate.

The computation of the probability ratio becomes unfeasible when one of the probabilities is zero. Consequently, for probabilities with values of zero, an alternative value of approximately zero is assigned. To serve as a substitute for zero, the value 1/1250 has been selected, because it is approximately an order of magnitude smaller than the smallest probability. An overview of all probabilities can be found in appendix B, table B.5 to B.8. This proxy value is consistently applied across all time periods. The confidence limits are estimated at 0 and 2/1250, respectively the lower and upper limits.

Bootstrap

The 95% confidence intervals are empirically estimated for the probabilities using a 200.000-member non-parametric bootstrap. The 2.5% and 97.5% percentiles are computed for the probability per data source. The confidence intervals are propagated with error propagation for the mean probability and the probability ratios.

4.3. Analysis and Synthesis

The last steps encompass analysis and synthesis of the results.

First, the results of the Regional Climate Models and the Global Climate Models are validated against the observations. A comparison is conducted between the timing of the individual events identified in the RCM data and the observational Ice core and Passive Microwave datasets. Additionally, the probabilities resulting from the RCM data are compared to the probabilities resulting from the observations. The validation of the CESM HR data is done by comparing the probabilities from the Ice core and Passive Microwave datasets to the probabilities from the CESM HR dataset.

The analysis encompasses first the analysis of the observational results. The observational probability ratios are combined into one probability ratio by taking the unweighted mean. The confidence interval is propagated for this mean. The analysis of the observations is followed by the analysis of the climate model simulation results. The probability ratios of the three climate model simulations are combined into one model probability ratio by taking the mean and propagating the confidence interval.

The results of the observations and climate models are synthesized into one probability ratio, in order to make a synthesized attribution statement. To calculate the synthesized probability ratio and its associated confidence interval, an unweighted average of the Observations PR and Models PR is taken. Given that there are four observational datasets contributing to the Observations PR, each individual dataset contributes 1/8th to the synthesized PR. Meanwhile, the Models PR comprises three model simulations, with each simulation contributing 1/6th to the synthesized PR.

5

Results

This chapter presents the research findings, which contribute to addressing both the main and sub-research questions. To begin, section 5.1 elaborates on the selection of thresholds for detecting melt events. The detection of melt events is a crucial step since all subsequent analyses depend on the identification of when these events occurred.

Following the results of the threshold selection, section 5.2 presents the analysis of observational results. This analytical process commences by analysing the detected events within the observational dataset. Subsequently, it scrutinizes probabilities and probability time series. These sections involve the validation of Regional Climate Models against observational data and offer insights into the current climate state and recent historical trends. The section culminates with an assessment of probability ratios, comparing the current climate with the pre-industrial period

Upon completing the analysis of observational results, the focus shifts to the climate model results, which offer valuable insights for attribution and future projections. This section includes the validation of the Global Climate Model through a comparison with observations and Regional Climate Models, evaluating probabilities and probability time series. After validation, it proceeds to analyze the probability time series for future scenarios, followed by an assessment of the probability ratios between various time periods. This entails comparing the probabilities found for the pre-industrial period with those found for the current and future periods.

The synthesis of probability ratios from both observations and climate models leads to the formulation of a consolidated attribution statement, as detailed in section 5.4.

5.1. Detection of melt events caused by Atmospheric Rivers

The following section outlines the thresholds that have been derived. In appendix C a description of the melt events detected using these thresholds can be found. Furthermore, in section 5.2 the events are analysed.

5.1.1. Threshold number of data points

In table 5.1 the thresholds for the number of data points needed to detect melt are displayed. The threshold for the number of data points needed to detect melt in the PM and CESM HR data is one pixel. The threshold for the MAR data is set to six pixels, covering an area of 600 km^2. Conversely, in the RACMO dataset, a total of 636 pixels are selected, covering a combined area of 636 km^2.

Data source	Threshold for # data points indicating melt	Area of one data point [km2]
CESM HR	1	461 or 1156
PM	1	625
MAR	6	100
RACMO	636	1

Table 5.1: The threshold for the number of data points indicating a melt event per data source.

5.1.2. Threshold amount of melt per data point

In table 5.2 the thresholds for melt at a data point are displayed. The results of the selection of the thresholds are elaborated on below.

Data source	Threshold x for melt at a data point	Unit	Per
CESM HR	0.08	mm	month
PM	1	-	day
MAR	2.3	mm w.e.	day
RACMO	0.8	mm w.e.	day

Table 5.2: Threshold for melt at a data point per data source

A first look at the RACMO and MAR data confirms the need for a threshold per pixel that is well-balanced. When analysing the melt values in the RACMO data, it strikes that almost all years have pixels within the AOI with melt, see figure 5.1. This is due to the high resolution of the RACMO data and underscores the need for a threshold per pixel. What can also be seen, is that the choice for the threshold per pixel has a big influence on the amount of melt events that are detected and thus on the resulting probability. The other reanalysis-forced RCM data used for this study, ERA-forced MAR data, shows similar results; a lot of pixels have a little bit of melt on many days, see figure 5.2. Therefore, similar to the RACMO data, setting a threshold for melt at a pixel is needed. However, the threshold choice strongly influences the results.

RACMO

The threshold for the RACMO data that results in the best comparison with the station data is $0.8\ mm\ w.e.$. This threshold is found, after considering several thresholds suggested by literature.

Fettweis et al. (2011) compared melt detection thresholds between RACMO, MAR and Passive Microwave data. They found that the best comparison occurs for a threshold of daily meltwater production of $8.25\ mm\ w.e.$ for the RCM. However, when this threshold is applied to the melt values at the Summit, no melt events are detected in the RACMO data (see figure 5.1), nor in the MAR data (see figure 5.2). For the MAR data, this discrepancy can be attributed to the warm bias present in older versions of the MAR model. This threshold is deemed not a good fit for this case.

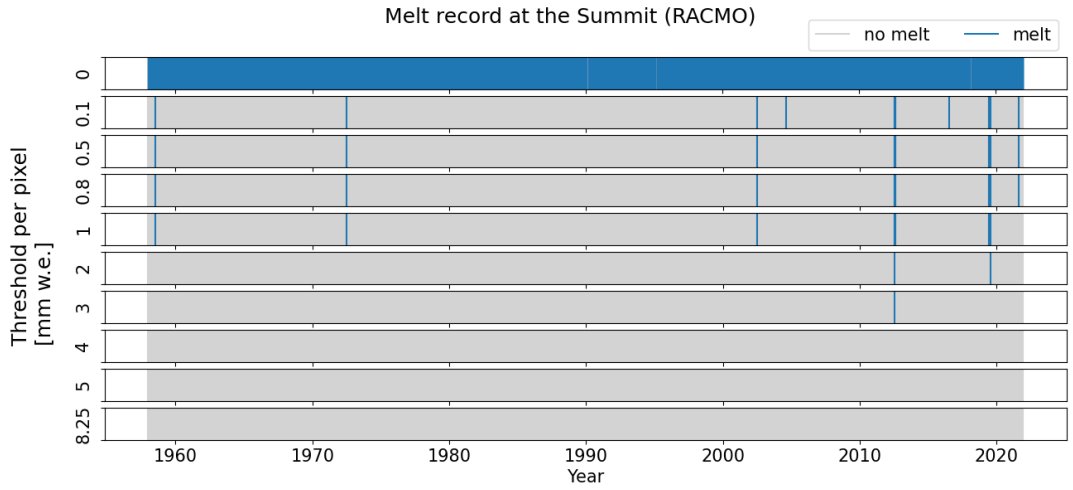

Figure 5.1: Melt record at the Summit (RACMO) for multiple thresholds. With blue bars melt events are indicated. The considered thresholds go from small (0 mm w.e.) to large (8.25 mm w.e.)

An expert in the field of RACMO data (Noël et al. (2021), Noël et al. (2018)) uses a threshold for melt at a pixel of $1\ mm\ w.e.$ per day (Noël, personal communication 2023). When this threshold is applied to the Summit area, seven melt events are detected, including melt events in mid-July 2012 and end of July 2019, as in the Summit station data. This is close to the results of the station data, however, ideally,

the August 2021 melt event is also detected. As shown in figure 5.1, when a threshold of $0.5\ mm\ w.e.$ or lower is used, the melt event in August 2021 is also detected.

The threshold is therefore sought between 0.5 and 1, with steps of 0.1. The highest threshold where the 2021 melt event is detected, is at $0.8\ mm\ w.e.$. This threshold, therefore, gives the best comparison with the Station data and is thus used for the RACMO data. The melt as modelled by RACMO for the dates where above melting temperatures were detected in the Summit Station data, are visualised in appendix A. Melt for 10-13 July 2012 can be viewed in figure A.3, melt for 30 July-2 August 2019 in figure A.4 and melt for 13-16 August 2021 in figure A.5.

MAR

Applying a threshold of $2.3\ mm\ w.e.$ results in the best comparison between the station data and the MAR data. ULiège and Fettweis (2023) use a threshold of $5\ mm\ w.e.$ to process ERA-forced MAR data real-time. When this threshold is applied to the melt data at the Summit, only one melt event is detected. This is not in line with the results of the Station data, therefore lower thresholds are explored. A threshold of $2\ mm\ w.e.$ results in melt events in 2012, 2019 and 2021, but also in a lot of other years in the period where there are no events in the Summit Station data. When a threshold of $3\ mm\ w.e.$ is applied, melt events in 2012 and 2019 are still detected, however, in 2021 no melt event is detected anymore. Therefore the threshold is sought between 2 and 3 mm w.e. in steps of 0.1 mm. A threshold of $2.3\ mm\ w.e.$ is the highest threshold where the 2021 melt event is still detected and therefore results in the best comparison with the station data.

What strikes in the MAR data, is that melt events appear in similar years as in the Summit Station data, however, the dates do not correspond. It is expected that the dates correspond, as the input for the MAR model is reanalysis data, which is veracious. The mid-July 2012 melt event is not detected at all in the MAR output, even when the threshold for melt is 6 pixels with zero mm w.e. of melt, this event is not detected. A spatial visualisation of the melt on Greenland during these days can be seen in appendix A figure A.6. This event is therefore not used as a reference to set the threshold for the MAR data. The end of July 2019 melt event does appear in the MAR output, this melt event can be seen in figure A.7. The third melt event, in August 2021, can be detected in the MAR output. However, this is only possible when the threshold for melt at a pixel is 1.3 mm w.e. or lower. This threshold would cause a lot more melt events to be detected over the whole period where MAR output is available, as well as in the period where Station data is available, which detected no other melt events. Therefore, the choice is made to not go with a threshold that detects the specific 2021 melt event, but to go with a threshold that detects melt events in similar years, but different dates. This is deemed to be a better fit with the Station data.

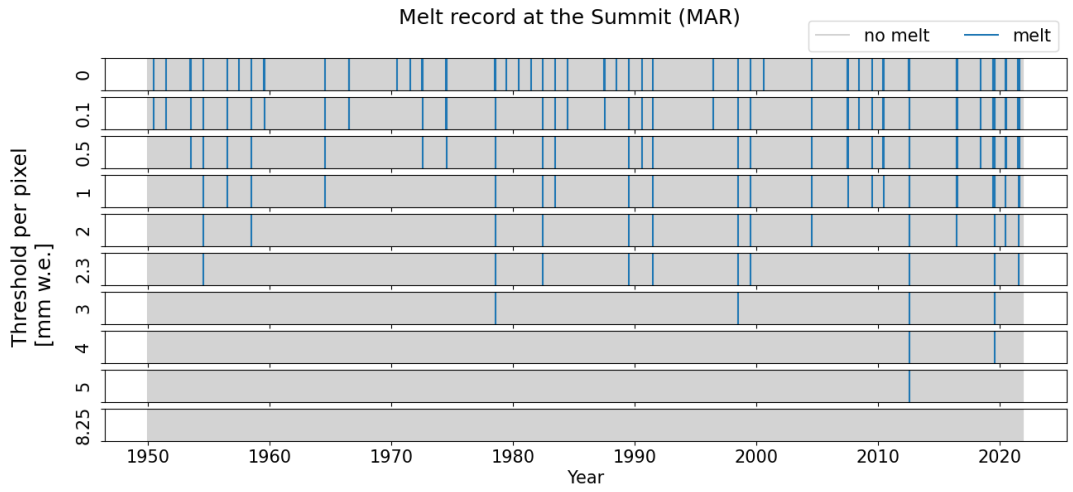

Figure 5.2: Melt record at the Summit (MAR) for multiple thresholds. With blue bars melt events are indicated. The considered thresholds go from small (0 mm w.e.) to large (8.25 mm w.e.)

CESM HR

The threshold that results in the best agreement between the three CESM HR ensemble members and the Summit Station data is $3e^{-8}\ mm/s$. The threshold is found by comparing multiple options, starting with the options $[0,\ 1e^{-9},\ 1e^{-8},\ 1e^{-7},\ 1e^{-6},\ 1e^{-5}]\ mm/s/month$. These thresholds are relatively small because the melt is present in the model data in small quantities as well. The melt events resulting from applying these thresholds are visualised in appendix A, in figure A.9, figure A.10 and figure A.11 of E1, E2 and E3 respectively. Based on a visual inspection of these figures, a new set of thresholds is studied. All thresholds between 0 and $1e^{-7}$ with steps of $1e^{-8}$ are considered. Based on a visual inspection, the threshold of $3e^{-8}\ mm/s$ is chosen as the threshold with the best agreement with the Summit Station data. This threshold results in three melt events between 2010 and 2020 and six melt events between 1990-2020 for Ensemble-member 1, two (three) melt events between 2010 (1990) and 2020 for Ensemble-member 2 and four (five) melt events between 2010 (1990) and 2020 for Ensemble-member 3.

To get an idea of how this threshold relates to the thresholds of the other data sources, the threshold is converted from mm/s per month to the total amount of melt in one month in mm. This results in a threshold of $0.08\ mm$ per month, however, it can be assumed that all melt happened on one day and therefore the threshold can also be interpreted as $0.08\ mm$ per day. When comparing this threshold to the other thresholds, it strikes that the threshold for the CESM HR data is an order magnitude smaller than the thresholds for the RACMO and MAR data. The reason for this difference could be in the spatial or temporal resolution differences.

5.1.3. Thresholds for Atmospheric River circumstances

The threshold for detecting Atmospheric River circumstances is set by summarizing the circumstances on the 3rd of September 2022 and the month of September 2022 in the GC-Net station data. The daily maximum, daily mean and monthly mean temperature and humidity are summarized in table 5.3. Next to this, the thresholds that arise from these circumstances are displayed.

Measure	**T [C]**		**Q [g/kg]**	
	Sep 2022	**Threshold**	**Sep 2022**	**Threshold**
Daily maximum	-2.015	-2.115	4.520	4.068
Daily mean	-3.632	-3.732	4.048	3.645
Monthly mean	-14.982	-15.082	1.868	1.681

Table 5.3: Thresholds for detecting AR circumstances derived from temperature and humidity data of September (3), 2022 from the GC-Net Station.

5.2. Analysis observations

In this section, the results of the observational data are presented. A comparison between the RCM and direct observations is made by analysing specific events, probabilities and probability time series. By analysing the probabilities, the current climate is described and the probability time series provide information about the recent past. This section ends with a description of the probability ratios, providing a comparison between the pre-industrial and current climate.

Specific Events

Figure 5.3 shows the specific events that were detected in the observational data sources with the thresholds as presented in section 5.1. The dates of the specific events are described in appendix C, section C.2 to C.5. The specific events found in the Ice Core data are not included in figure 5.3, they are described in section C.1.

The reanalysis forced regional climate model results are tuned such that the results are in line with the results from Summit Station data. The years with melt in the RCM results are aligned with the years with temperatures above zero in the Station data. By looking at figure 5.3 it can be confirmed that the timing and number of events align quite well for the last decade. A more elaborate comparison can be found in section 5.1.

When the Passive Microwave observations are included in the comparison, it strikes that the RACMO and MAR results align quite well with the PM results too. The RACMO and PM results agree on four specific melt events. There are two melt events that are in the PM results, but not in the RACMO results and two melt events that are in the RACMO results (within 1980-2021), but not in the PM results. When comparing the events found in the MAR results to the Passive Microwave results, it strikes that only one event can be found in both data sets. The years of melt, however, match reasonably well with each other. What stands out in the MAR results, is that there are seven events prior to 2010, whereas the PM results show only two events prior to 2010.

Specific events found in the ice core data in recent times encompass only a melt event in 2012. This melt event is detected also in the PM results as well as in both RCM results.

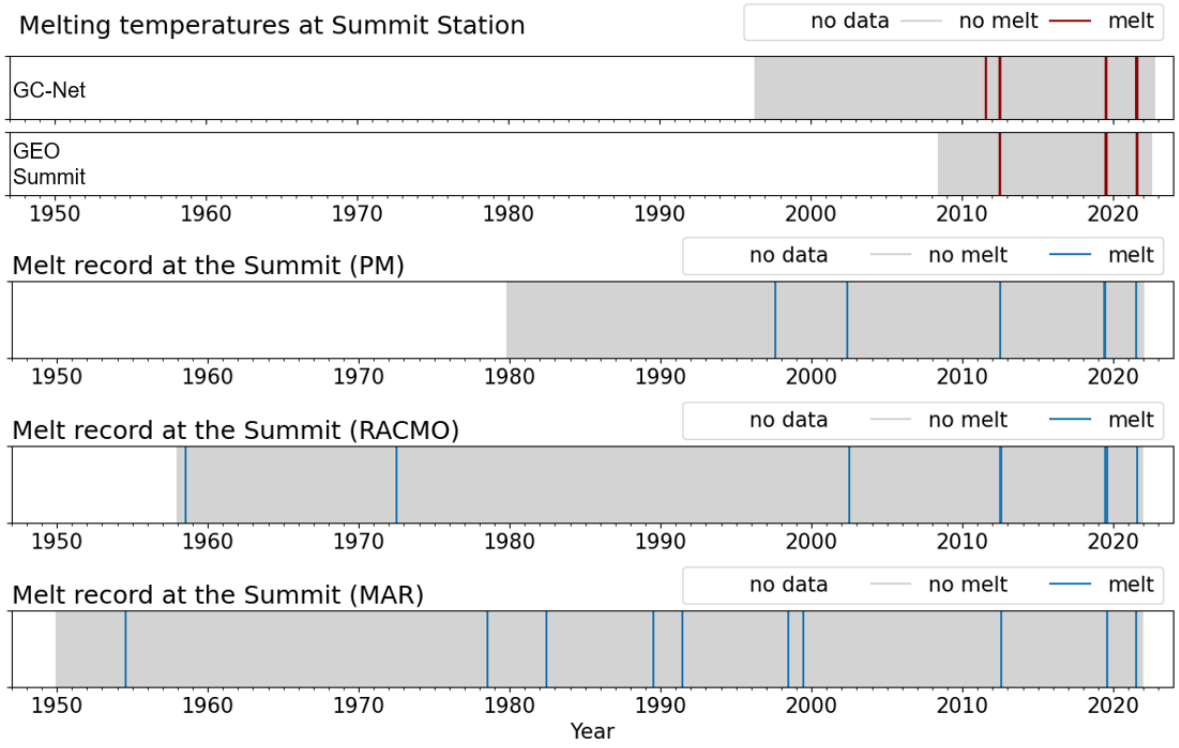

Figure 5.3: Detected melt events in station data, PM, RACMO and MAR with the selected thresholds

Notably, not all melt events identified in the observational data coincided with the presence of Atmospheric River (AR) conditions in the station data. Specifically, when considering the PM results, it

was determined that 65% of the days with melt were accompanied by AR conditions. In the case of the MAR results, this percentage stood at 67%. In contrast, the RACMO results indicated that AR conditions were detected on all days with melt. However, it's important to exercise caution when interpreting these percentages, as these AR melt events form only a limited percentage of the total amount of AR events. These percentages amounted to 41% for PM, 37% for RACMO, and 15% for MAR results, as detailed in Appendix B, table B.1.

These figures suggest that the proportion of melt events caused by AR, similar to the September 2022 event, is lower than the overall count of melt events. When calculating melt event probabilities, all melt events are taken into account, not solely those with AR conditions. This approach ensures a fair comparison with the climate model data, where AR conditions are challenging to ascertain, and all melt events are considered as well.

Probabilities

Figure 5.4 displays the probabilities derived from all observational data sources, for the pre-industrial (PI) period (<1900) and current period (1990-2020), for the month of September as well as for any month. The probability is the probability of a year with melt.

For the month of September, it becomes clear that all sources indicate a probability of approximately zero. This is because no melt events were detected in the period of interest. These results are in line with the literature (Moon et al. (2021), NSIDC (2022)), which indicates that the September 2022 melt event was the first time melt was detected at the Summit since observations started. The mean probability of a melt event in September according to observations is approximately zero: $p_{Sep} \to 0$.

To get a broader view of how rare the September 2022 melt event was, the probability of a melt event in any month during the year is computed for all data sources as well (see figure 5.4). The first thing that strikes, is that the probability based on the direct observations, the ice core data and the PM data, differ by 0.10. This difference is large compared to the order of magnitude of the probabilities themselves, which is also around 0.10. The probability derived from the RACMO data lies in between the PM and ice core results, 0.03 below the PM result. The probability derived from the MAR data lies 0.03 above the PM result. The combination of the four probabilities leads to a probability of melt in any month in a year for the period 1990-2020 of $p_{Any} = 0.117$ (95% CI, 0.065 to 0.180).

It should be noted that these numbers are based on only four data points, which is very little data. The result would be more reliable if more data sources can be added to the analysis.

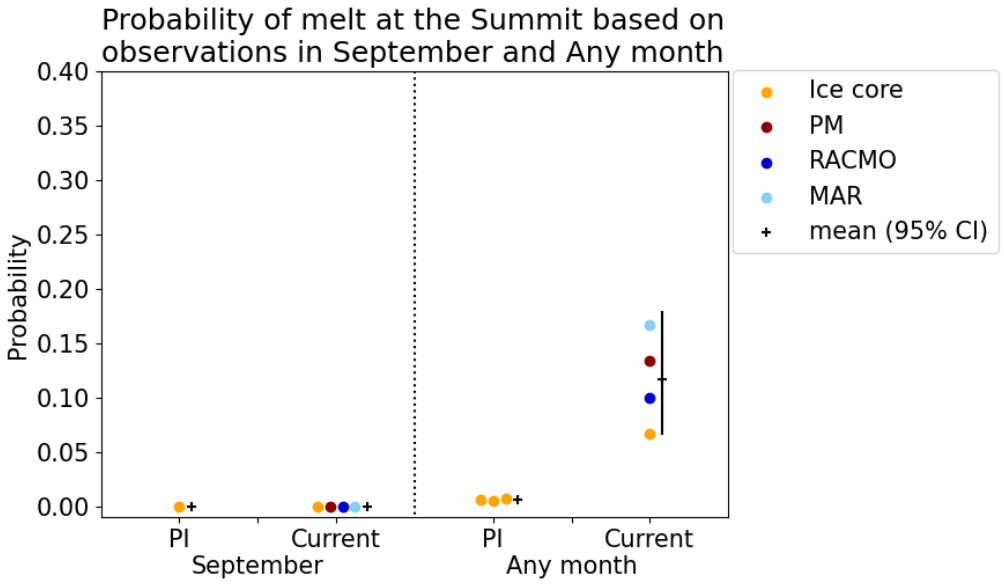

Figure 5.4: Probability of melt occurring at the Summit in September and in Any month, for the pre-industrial period (PI) and current period (Current). The mean and 95% confidence interval of all observations per period are included. Exact values can be found in table B.5 and table B.6

Probability time series

In figure 5.5 the probability time series of the Passive Microwave results, ERA-forced RACMO results and ERA-forced MAR results are shown. The time series are computed following the method described in section 4.2. The probability time series only have values until 2006, because 2006 is the centre year of the most recent period, namely 1991-2021. The time series for September are represented by dotted lines, and the time series for Any month are represented by solid lines.

The probability time series for September are zero for all years and all data sources. The results based on three data sources all agree, therefore, a melt event in September in the recent past was very unlikely.

When analysing the time series for Any month, it strikes that the probability derived from the RACMO data is low for most years and increases from 1996 onwards. The increase is parallel to the increase that the Passive Microwave data shows. However, the Passive Microwave data has no information on the years before the increase. When looking at the MAR data, it strikes that the probability of melt is overall higher than for both the Passive Microwave data and the RACMO data. Around 1970 the probability of the MAR data is on a similar level as the other two data sources, but after 1973 the probability increases. This increase lasts until 1984 and after 1992 a slight decrease seems present. This results in a similar probability of melt in 1991-2021 for MAR and PM and a slightly lower probability for RACMO. So, although the events of the station data are aligned with the events in the RACMO and MAR data, it appears that the time series of MAR deviates considerably from the time series of the PM and RACMO results.

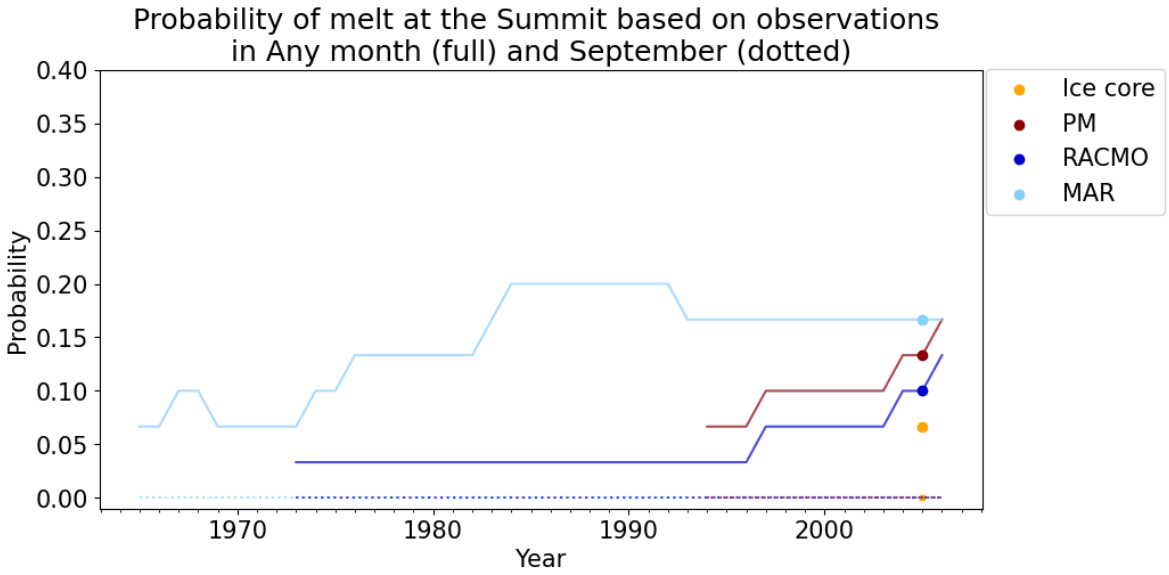

Figure 5.5: Probability of melt at the Summit based on Passive Microwave (PM) observations, ERA-forced RACMO data (RACMO) and ERA-forced MAR data (MAR) in any month (full line) and in September (dotted line). Probability computed over 30-year intervals with 1-year increments. The dot represents the probability for 1990-2020.

Probability Ratios

The probabilities determined from observations are combined into probability ratios (PRs). These probability ratios pertain to the Current period (Current versus Pre-Industrial period) for the month of September, and they are visually represented on the left side of figure 5.10. Similarly, probability ratios for Any month are illustrated on the right side of figure 5.10. The individual probability ratios per observational data source are depicted in light blue while the mean of all observational probability ratios is presented in medium blue. A PR value exceeding 1 signifies an increase in probability, whereas a PR value below 1 indicates a decrease in probability. When the confidence interval encompasses the PR value of 1, the observed change is considered statistically insignificant. For the precise PR values, please refer to the Appendix, tables B.11 and B.12.

For the month of September, all PRs resulting from observational data are at a value of 1.00 (95% CI, 0.00 to 2.41). This uniformity arises from the fact that probabilities in both the pre-industrial and

current periods are approximately zero for all data sources. The mean of these PRs also stands at 1.00 (95% CI, 0.29 to 1.71), signifying no discernible shift in the likelihood of melt occurrences in September when comparing the pre-industrial and current climate, as indicated by the observational data.

The PRs for Any month exhibit a broader range, spanning from 10.79 to 26.97. The lower confidence boundary of the PRs of RACMO and the Ice core data is 0.00, and therefore the confidence interval encompasses the value of 1, which indicates an insignificant PR. The lower confidence boundaries of PM and MAR PRs are above 1, approximately 3. The mean PR across all observations stands at 18.88 (95% CI, 9.62 to 31.51). This suggests that the probability of experiencing melt conditions at the Summit during any given month throughout the year is approximately 19 times higher in the current climate compared to the pre-industrial climate. While this value comes with a level of uncertainty, the lower confidence bound well exceeds 1, indicating a statistically significant positive change in probability.

5.3. Analysis climate models

The results of the probability and probability ratio computations on the climate model data are presented in this section. The specific events that underlie these computations and that resulted from the melt detection, are described in appendix C, section C.6. The probability computations were done for the current climate, the pre-industrial climate and the future climate considering all months together as well as the month of September separately. To evaluate the climate model results, a comparison with observations is made. Lastly, the probability ratios based on the climate model results are presented.

Atmospheric River circumstances

Before the probabilities of melt events in climate model data are analysed, first it is examined whether Atmospheric River circumstances were present during these melt events. To establish this, the monthly mean temperature and humidity data in the climate simulations are compared to those of September 2022.

In the pre-industrial run, all four detected melt events coincide with AR circumstances. However, these events constitute only 1% of the total of 351 AR events detected in the pre-industrial data. Consequently, the overall agreement between melt and AR circumstances appears to be quite low.

Similar patterns emerge from the historical run, where AR circumstances are detected during 86% to 100% of the melt events. Nonetheless, these melt-associated AR events represent only 4% to 6% of all detected AR events, making it less impressive that these months share such conditions. Notably, in the historical run, it's striking that the two melt events detected in September lack AR circumstances. This may indicate that these melt events were not caused by AR and thus were dissimilar to the September 2022 event. However, drawing firm conclusions remains challenging given the monthly data.

In the future run, there is a reasonable overall agreement between melt and AR circumstances. Between 70% and 100% of the melt events in the three ensembles exhibit AR circumstances, constituting 23% to 33% of all detected AR events. Furthermore, unlike the historical run, the future run does not exhibit a distinct difference between the September events and other months.

The detection of AR circumstances is solely used to provide context and is not utilized for selecting melt events for probability calculations. All melt events are considered in these calculations.

Probabilities

Figure 5.6 displays the resulting probabilities based on PM observations, Ice core observations, RACMO data, MAR data and Global Climate Model runs all together. The probabilities for the pre-industrial, current and future climate are displayed for both September and Any month. The exact numbers of the probabilities can be found in appendix B, table B.5 to B.10.

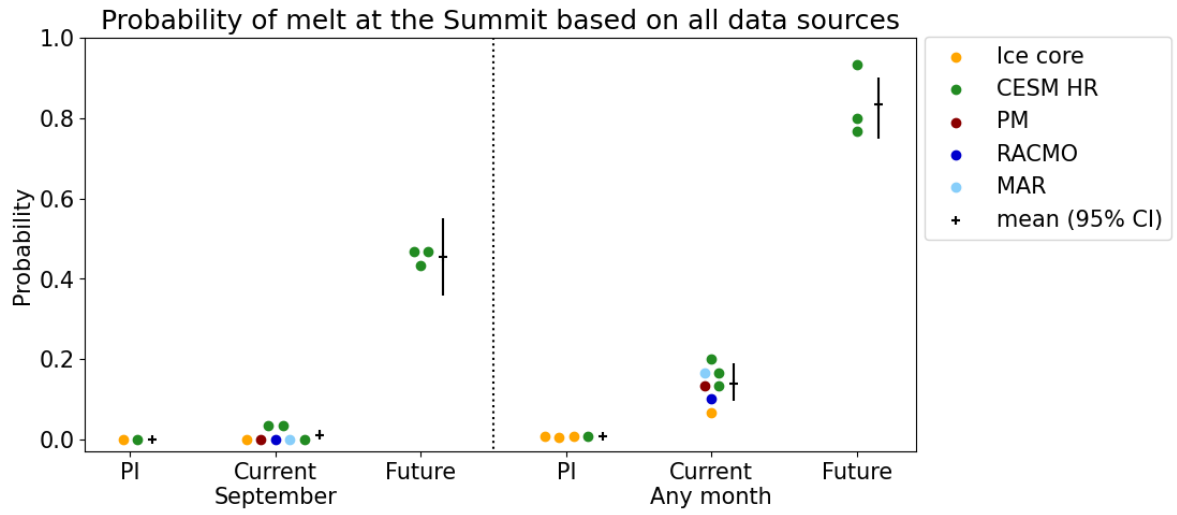

Figure 5.6: Probability of melt at the Summit based on all data sources. For September as well as for all months. Exact values can be found in table B.5 to B.10

The CESM HR results are calibrated to align with the results from Summit Station data over the period 1996-2021. In the current section, a comparative analysis is conducted between the CESM HR results and the findings from Passive Microwave and Ice core measurements as well as the Regional Climate Models. This comparison serves two purposes: evaluating the model simulation and determining whether the model simulations can be utilized to make predictions regarding the likelihood of melting events at the Summit in the future.

For melt events in the month of September in the pre-industrial climate, the ice core results as well as the CESM HR results show no melt events in September and thus a probability of approximately zero: $p_{Sep\ CTRL} \rightarrow 0$. This is in line with the expectations. The probabilities resulting from the CESM HR simulations for the current period show some spread but are comparable to the observations. One ensemble member shows no melt, similar to the observational and reanalysis-forced RCM results. Two ensemble members detect one melt event in the simulations for 1990-2020. This results in a mean model probability of $p_{Sep\ HIST}$ = 0.022 (95% CI, 0.007 to 0.054).

The probabilities for a melt event in any month in the pre-industrial climate are very comparable between the Ice core data and the CESM HR data. The probability from the model results is one over 125: $p_{All\ CTRL}$ = 0.008 (95% CI, 0.002 to 0.016) and the probabilities of the Ice core data are between one over 150 to 187.5. Thereby it seems like the climate model is able to capture the melt event frequency in the pre-industrial climate. The results for the current climate show a larger spread. For the melt events in any month, the probabilities can be found between 1/15 (Ice core) and 1/5 (CESM E1), with the mean of the model simulations at 1/6: $p_{All\ HIST}$ = 0.166 (95% CI, 0.101 to 0.250). It strikes that the probabilities from the CESM HR data compare well with the probabilities determined from the PM, RACMO and MAR data, however, they are two to three times larger than the Ice core probability.

Probability time series

Next to the probabilities for the pre-industrial and the current climate, the probability time series of the recent past are compared as well. Figure 5.7 shows the mean probability time series derived from the CESM HR simulations as well as the time series obtained from the PM, RACMO and MAR data. The time series for Any month are shown in solid lines and the time series for September are shown in dotted lines.

The time series extracted from CESM HR simulations for the month of September exhibits non-zero values, in contrast to observations of the recent past for September. Starting From the beginning of the simulations until the mid-1980s, the probability is zero. However, from that point onward until 2006, which also marks the conclusion of the observational time series, the probability has increased to 0.011. This alignment suggests a reasonable comparison between the model and observational time series. Subsequently, after 2006, the probability remains within the range of 0.011 to 0.022.

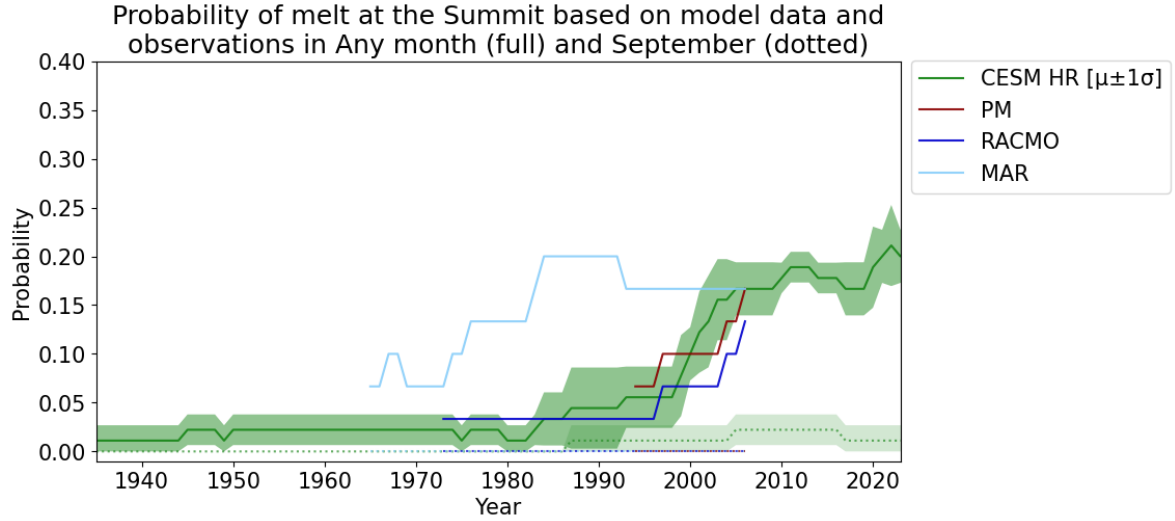

Figure 5.7: Probability of melt at the Summit in any month based on CESM HR data, PM observations and RCM data displayed for the recent past (1920-2008). The control run is shifted in time and shown as a reference. For CESM HR: the line represents the mean and the shaded area represents 1 std from the mean.

When looking at the time series for Any month (solid lines), the CESM HR time series compares reasonably well with the PM and RACMO time series, all three both show an upward motion over the period 1996-2006. The probabilities of the CESM HR simulations are at first, until the end of the 90s, in agreement with the RACMO results and slightly below the probabilities of the PM data. However, from 2000 onwards the probabilities of the CESM HR data rose above the probabilities of the PM data and far above the probabilities of the RACMO data. Around 2006 the probabilities of CESM HR and PM align and end slightly higher than the RACMO results. The MAR time series does not compare well with the CESM HR as well as the other time series. The MAR time series is far above the CESM HR time series and only from 2001 onwards, the probabilities are comparable.

The probabilities and probability time series show reasonably well agreement with the observations and reanalysis forced RCM, therefore the CESM HR simulations are used for the analysis of the coming century until 2100.

Probability time series - future

In figure 5.8 the probability time series of melt at the Summit for the coming century are displayed in green for September (dotted lines) as well as for Any month (solid lines). The mean and standard deviation (fixed values) of the control simulation are displayed in orange for both September and Any month. The control simulation represents the pre-industrial period.

When looking at the Historical + Future time series for September, it strikes that, after the departure from 0 in the mid-1980s, the probability remains between 0.011 to 0.022 until 2040. From 2040 onwards, the probability departs permanently from the control simulation and increases until a value of 0.456 (95% CI, 0.360 to 0.552) by the end of the time series in 2085. The control simulation has a constant value of 0.00.

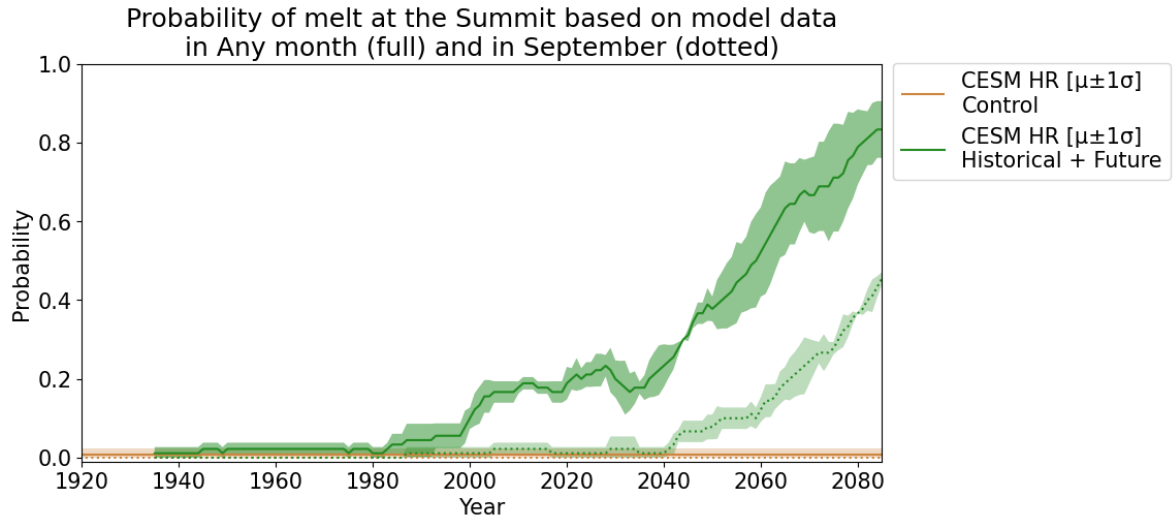

Figure 5.8: Probability of melt at the Summit in any month and in September based on CESM HR data, displayed for the past and the future (1920-2085). The control run is shifted in time and shown as a reference. The line represents the mean and the shaded area represents 1 std from the mean.

When looking at the Historical + Future simulation of all months together, it strikes that the increase in probability started already in the recent past. From 1980 onwards small and large increases in probability are present. From 1982 onwards, the mean of the Historical + Future simulations is outside the 1σ upper boundary of the control simulation. From 2000 onwards, the 1σ lower boundary of the Historical + Future simulations also departs from the 1σ upper boundary of the control simulation, meaning that all simulations are outside the natural variability of the pre-industrial climate. Around 2005 the probability of the Historical + Future simulation stabilizes at around 0.2 until 2035. From 2035 onwards a vast increase in the probability is present. By the end of the time series, the probability has risen to a value of 0.832 (95% CI, 0.748 to 0.900). The start of the increase in probability coincides with the increase in probability for September. From that moment onwards the causing factors for melt events seemed to have increased enough to cause more and more melt events in general, of which an increasing part

happens in September.

Probability Ratios - current

The probabilities derived from the model simulations are combined into probability ratios (PRs) that pertain to the Current period as well as the Future period for both September and Any month. Each CESM HR ensemble member's PR is individually calculated and depicted as a light pink bar, which is then aggregated into a mean value represented by a dark pink bar. For the precise PR values, please refer to the appendix, tables B.11 and B.12.

Figure 5.10 illustrates on the left side the PRs for the Current period for the month of September. What stands out is the considerable variation among the CESM HR ensemble members. Two ensemble members exhibit a PR of approximately 40, while one member exhibits a PR of 1. This difference originates from the absence of melt events in September during both the pre-industrial and current periods. In the pre-industrial simulation and ensemble member 3, no melt events occurred, resulting in a probability of zero. In contrast, ensemble members 1 and 2 had one event during the current period. Given that 1 event in 30 years is approximately 40 times larger than $\rightarrow 0$, this stark contrast occurs. The mean PR is 28.11 (95% CI, 0.33 to 72.00), indicating a non-significant positive change in probability.

Figure 5.10 presents on the right side the PRs for the Current period for Any month. In this case, the PRs exhibit greater similarity, falling within the range of 16.67 to 25.01, suggesting an overall increase in probability. Nevertheless, it's worth noting that the confidence intervals for all three ensemble members encompass the range from 0 to 1, rendering them individually non-significant. However, when these individual values are combined to calculate a mean PR, the resulting confidence interval substantially exceeds 1. Specifically, the mean PR is 20.38 (95% CI, 8.08 to 36.92), indicating statistical significance at this aggregated level.

Probability Ratios - future

The results from the CESM HR model simulation can also be applied to calculate probability ratios for the future period relative to the pre-industrial period. In Figure 5.9, the probability ratios specifically for the month of September are presented on the left side. All three ensemble members exhibit similar and exceptionally high PRs, ranging from 541.67 to 583.33, resulting in a mean PR of 569.44 (95% CI, 219.16 to 919.64). This remarkably high probability ratio arises from the approximately zero probability in the pre-industrial period compared to an almost 50% probability in the future period. Notably, it's worth mentioning that the individual confidence intervals for the ensemble members are wide and encompass 1, signifying that the change in probability is not statistically significant despite the elevated PR values. However, when these values are aggregated into a mean, the lower boundary of the confidence interval substantially exceeds 1, indicating a significant PR at this combined level. The magnitude of this PR is disputable since it is heavily dependent on the choice for the approximately zero value. Nevertheless, a PR greater than 1 is highly probable.

Figure 5.9 displays on the right side the probability ratios for the future period for Any month, these PRs can be substantiated with a more substantial number of melt events. These PR values indicate a mean value of 104.17 (95% CI, 57.68 to 165.21). The lower boundary for all ensemble members is significantly greater than 1. This indicates a significant shift in the probability of melt occurrences at the Summit in any month during the year in the future.

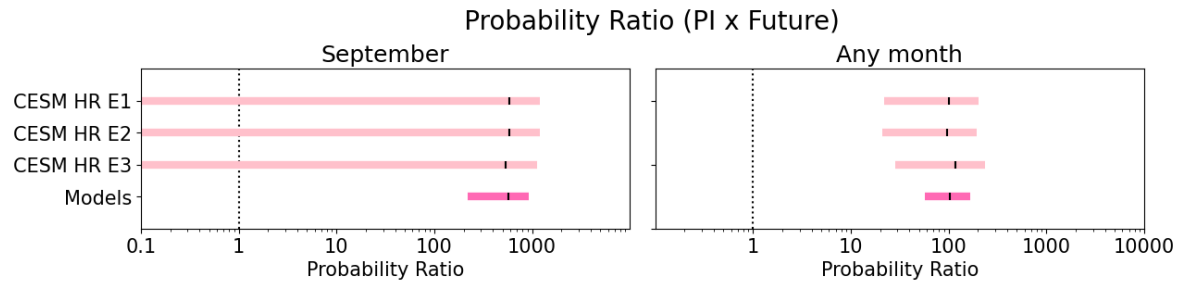

Figure 5.9: Probability Ratio between the pre-industrial (PI) and Future period for the month of September (left side) and for Any month (right side) based on the CESM HR model simulations. The PR is shown as a black line, the coloured bars represent the 95% confidence intervals. Exact values can be found in table B.11 and table B.12

5.4. Synthesis observations and models

In this section, the synthesis of the observational and model results is presented. This synthesis incorporates all available observational datasets and model simulations analyzed in this paper.

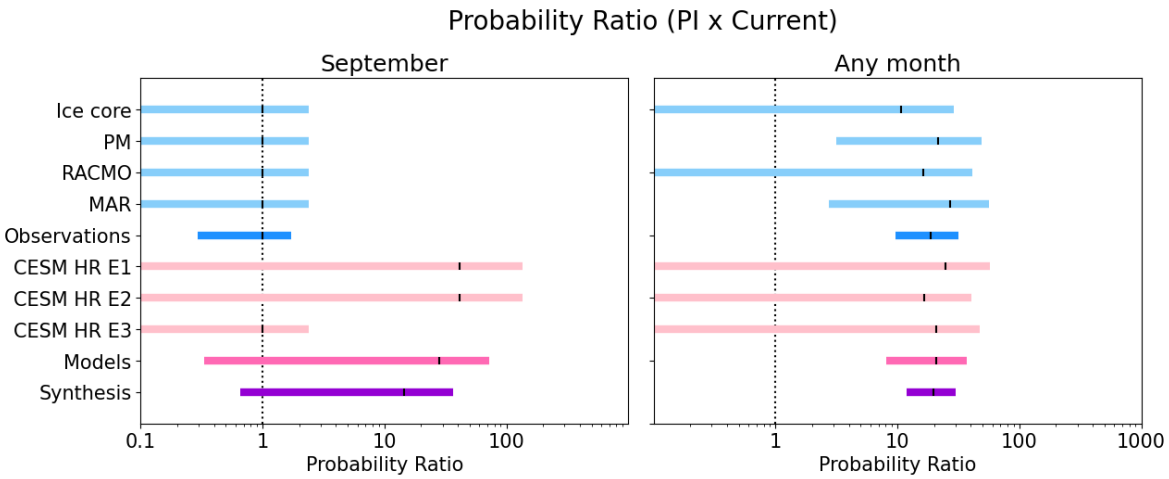

Figure 5.10: Probability Ratio between the pre-industrial (PI) and Current period for the month of September (left side) and for Any month (right side). The PRs are based on observations and model simulations. The PR is shown as a black line, the coloured bars represent the 95% confidence intervals. Exact values can be found in table B.11 and table B.12

The synthesis results are depicted in figure 5.10, where the September results are presented on the left side. Notably, the PR of the observations stands at 1, while the models exhibit a PR of 28. When combined, these values yield a synthesised PR of 14.56 (95% CI, 0.66 to 36.50), signifying a notably high PR. However, it is important to note that the Confidence Interval includes the value 1, indicating that the observed change is not statistically significant. This wide interval results from the limitations imposed by the limited data availability. Consequently, it is appropriate to conclude that, although a high probability ratio is found, no definitive attribution statement can be made regarding melt at the Summit in September.

Regarding melt events throughout the rest of the year, a more extensive dataset becomes available. Consequently, a synthesis of the Probability Ratios (PRs) for melt in Any month of the year has been conducted. Notably, the PR stemming from observations stands at 18.88, exhibiting a modest deviation of merely 2 from the PR derived from the models, quantified at 20.83. When amalgamated, they yield a PR of 19.86 (95% CI, 11.98 to 30.08). The lower boundary of this confidence interval significantly exceeds the threshold of 1, attesting to its statistical significance. Consequently, if an event akin to the melt event observed in September 2022 were to transpire in another month, a reasonable assumption would be to attribute it to anthropogenic climate change. This attribution only holds under the assumptions made in this analysis and caution should be exercised in its interpretation, given the inherent constraints of a limited data set and a lack of diverse models.

The future risk ratios are not subject to synthesis in this context, because only one model, encompassing three simulations is considered. These simulations have already undergone comprehensive analysis in section 5.3.

6

Discussion

In this chapter, some of the issues encountered during this research are discussed. Additionally, the results are interpreted in the light of uncertainties.

Attributing the extreme melt event of September 2022 to human-induced climate change, the main objective of this study, proved to be a challenging endeavour. The Event Attribution Protocol by Philip et al. (2020), which is typically employed for such analyses, was found to be less suitable for this particular event. This was primarily due to the limited occurrences and small amounts of melt at the Summit, which led to the melt variable exhibiting binary characteristics. The inherent binary data made it impossible to fit an extreme value distribution, rendering the determination of return times and probabilities unfeasible through this approach. Consequently, the protocol by Philip et al. (2020) could not be used and a simpler and less robust methodology had to be adopted.

It became apparent that an alternative event definition might have yielded different results. For instance, investigating a different variable, such as temperature, might have been a viable option. Temperature data offers a continuous range of values, in contrast to the binary nature of the melt variable, enabling the fitting of an extreme value distribution. However, this approach would have required making assumptions about the relationship between temperature and melt, a task not devoid of complexity but potentially fertile ground for future research.

Another possibility could have involved expanding the geographical scope to encompass lower-lying regions. This expanded spatial coverage would have yielded a greater volume of melt data, thereby mitigating the binary nature of the variable and facilitating the application of the Event Attribution Protocol. However, this option would have required making intricate assumptions about how the conditions in this larger area correlate with those at the Summit during an extreme melt event.

In the context of this research, the event was defined as melt at the Summit, which closely aligned with the study's focus. Detecting similar melt events necessitated the establishment of diverse thresholds. The selection of these thresholds for melt event detection wielded substantial influence over the outcomes, particularly with regard to the resulting probabilities. A minor adjustment in the threshold used for detecting melt events could result in a substantial alteration of the resulting probability. This influence introduces an element of uncertainty into the results, underscoring the importance of meticulous threshold selection.

In addition to the thresholds applied for melt detection, the process of Atmospheric River (AR) detection also encountered its share of uncertainties. While temperature and humidity serve as indicators of AR presence, the spatial characteristics play a pivotal role in AR detection. These spatial characteristics could not be studied due to the data limitations in this study, thereby limiting the effectiveness of the AR detection method. The inclusion of data from other sources, such as the Atmospheric River Tracking Method Intercomparison Project, could potentially address these limitations.

Furthermore, it's important to note that AR events typically manifest on an hourly to daily scale, a level of detail that station data effectively captures but is absent in the monthly resolution of the climate model data. This limitation significantly constrains the ability to detect AR events in the model data.

Given these constraints, the results of AR detection are utilized solely for providing context and are not employed in event selection. The omission of AR circumstances from the event selection process narrows the scope of conclusions that can be drawn in this attribution study, as not all melt events occurred under similar conditions as the September 2022 event.

The results of this study hinge on data drawn from four observational sources and four simulations from one climate model. While these sources provide valuable insights, it should be acknowledged that the quantity of available data imposes limitations on the certainty of the results. Next to the limited amount of observational data sources, it should be noted that the time spans are relatively short, from 40 years PM data up to 70 years MAR data. Ideally, a homogeneous time series of at least 150 years is available. For the climate models, the time spans of 180 to 500 years are sufficient.

Expanding the scope of observations holds the potential to enhance the depth and accuracy of the analysis, however, this is hard to realize. One promising avenue for improvement could involve employing RCM forced by a different reanalysis dataset like MERRA-2. Additionally, increasing the number of models could significantly improve the analysis. An expanded pool of GCM simulations is accessible through CMIP6 or initiatives like the HighResMIP, a coordinated set of High-Resolution model experiments, offering a promising means to advance the analysis.

A limitation inherent to the global climate model employed in this study pertains to its temporal resolution, which operates on a monthly basis. This choice likely represents a trade-off to accommodate the model's high spatial resolution. Nonetheless, this temporal resolution limits the possibilities and accuracy of the analysis that can be conducted. Ideally, a higher temporal resolution would be preferable, enabling the examination of melt events and atmospheric river circumstances on a daily scale.

A potential source of bias in the results stems from the calibration of the melt detection thresholds. The thresholds for both the RCM and GCM have been fine-tuned to align with the observational data. Subsequently, an assessment of the RCM and GCM results against observational data has been conducted. While this alignment with observational data serves to enhance the accuracy of the model results, it should be acknowledged that it may introduce a certain level of bias towards the station data results. This consideration should be borne in mind when interpreting the findings of this study.

An intriguing contradiction emerges when analyzing melt probability in September in the current climate. The complete absence of recorded melt events in observations starkly contrasts with the reason for this study, a melt event observed in September 2022. The rationale behind the absence of this melt event in the results of the current period stems from the fact that September 2022 falls outside the specified definition of the 'current period,' which encompasses the years 1990 to 2020. This choice is influenced by two primary considerations. Firstly, practical constraints play a considerable role, as almost no data source had data available for the year 2022. Secondly, this decision is taken to prevent any potential bias towards the extreme event, as the analysis would not have been done without it. However, it is acknowledged that valuable information gets lost by excluding the event of interest from the definition of the 'current period'. This is in line with previous studies (Philip et al., 2020).

In the recent past an upward trend becomes apparent in the amount of melt events on Greenland, corroborated by AMAP (2021). Substantial evidence points to recent increases in the frequency and intensity of various extreme events in the Arctic, including extreme high temperatures (Moore, 2016), as well as widespread melt events on the Greenland Ice Sheet (AMAP, 2021). Moreover, there is a noticeable uptick in circulation patterns characterized by robust poleward heat and moisture transport. These patterns are occurring with greater frequency, consequently leading to heightened instances of warm extremes in the Arctic (Vihma (2017) and Messori et al. (2018)).

The results for the future period rely on a single climate model, a limitation previously discussed in this study. This particular climate model projects future scenarios in accordance with Representative Concentration Pathway 8.5 (RCP8.5), one of four commonly used pathways for modelling future climate conditions. RCP8.5 is characterized as the scenario with the highest greenhouse gas emissions and the most substantial temperature increase, yet it remains a plausible scenario. A recent study suggests that RCP8.5 will remain a close match to emissions until the mid-21st century under current policies

(Schwalm et al., 2020). This insight should guide the interpretation of the results for the coming century.

In the simulations of future climate, a noticeable upsurge in melt events becomes apparent. This surge in melt aligns with the broader trends outlined in existing literature (AMAP, 2021). Notably, Hanna et al. (2021) suggests a substantial temperature increase of $4.0 - 6.6°C$ across Greenland under the SSP5-8.5 emissions scenario, resulting in significant surface melt. Furthermore, Collins et al. (2013) projects a rise of $5 - 7°C$ in the highest daily maximum temperature for Greenland by the end of this century, intensifying temperature extremes and consequently contributing to heightened melt occurrences. Moreover, the literature highlights an increase in Atmospheric River (AR) frequency of 50% in the Northern Hemisphere under the RCP8.5 scenario (Espinoza et al., 2018), a trend supported by Payne and Magnusdottir (2015). While this suggests the potential for a greater frequency of melt events if AR trends extend to Greenland, it's essential to note that specific AR trends for Greenland are currently unavailable. Nevertheless, despite the supportive evidence from existing literature regarding the factors driving melt events, accurately quantifying the precise magnitude of this increase remains a formidable challenge. Hence, it is paramount to approach the results of this study with a critical perspective, taking into account the inherent uncertainties and intricacies involved in such estimations.

7

Conclusions & Recommendations

The aim of this research is to study the influence of human-induced climate change on the September 2022 melt event through an attribution study and to assess the likelihood of similar occurrences in the future. The novelty of this research lies in attributing the recent September 2022 melt event. Understanding this extreme melt event, its causes, and future changes in the frequency of similar events can advance broader knowledge of climate extremes in Greenland, contributing to the development of climate mitigation and adaptation strategies. This research involves defining the characteristics of the melt event, detecting similar events in observational data and climate model simulations, calculating event probabilities and probability ratios, and synthesizing the results. In line with the research aim, the sub-questions are systematically addressed, leading to the resolution of the main research question. Lastly, recommendations for future research are presented.

7.1. Conclusions

How can melt events similar to the September 2022 melt event be detected in observations and model simulations?

Melt events similar to the September 2022 event are identified by setting a threshold to the melt variable from each data source. The threshold for detecting melt events is calibrated to align with the results observed at the Summit station. A threshold is set on the area indicating melt and the amount of melt per pixel. It's important to note that even a minor adjustment in these thresholds can significantly impact the resulting probability. Consequently, the accurate determination of appropriate thresholds is a crucial aspect of this study, however, the thresholds introduce a degree of uncertainty. Additionally, the Atmospheric River circumstances that could lead to these events are identified. Atmospheric river circumstances are identified when temperature and humidity levels exceed those observed during the September 2022 event. These thresholds are not utilized in the event selection process.

In the station data, a melt event is detected when the temperature rises above -0.1° C. A melt event is detected in the CESM HR data when one pixel shows 0.08 mm melt in a month, an event is detected in the PM data when one pixel has a value of 1 on one day. In the MAR data a melt event is detected when six pixels show 2.3 mm w.e. melt on a day and for the RACMO data when 636 pixels show 0.8 mm w.e. melt on a day.

How rare was the melt event in the current climate based on observations?

Melt events in September at Greenland's Summit have never been observed before, according to the observations included in this study. Such occurrences were absent both in the pre-industrial period and in the current period (excluding 2022). This singular fact alone underscores the remarkable rarity of this event. A melt event at the Summit in any other month of the year, thus not specifically in September, is infrequent, but not as exceptional as an event in September. The probability of observing a melt event at the Summit in any given month stands at 11.7%, a figure 19 times greater than the mere 0.6% probability associated with the pre-industrial period. A first examination of the AR cir-

cumstances suggests that considering these conditions could potentially result in fewer events being detected. However, this aspect cannot be definitively confirmed. Collectively, these findings lead to the conclusion that the September 2022 melt event was extraordinary within the context of the current climate.

How has the rarity of the melt event changed over the recent past, based on observations?

The transition in probability from the pre-industrial period to the present is clear-cut when considering September melt events. A constant probability of zero is observed in all available data. It is plausible that the probability is zero for all intervening years between the pre-industrial period and the start of the observational data in 1965. However, when examining melt events occurring in other months of the year, making such assumptions is more complex. The probability time series indicates a steady probability around 5% until the mid-90s, after which an upward trend suggests an increasing likelihood. While drawing conclusions for the intervening years between the pre-industrial period and the start of the observations is challenging, ice core data indicates minimal events during this time. Hence, it can be assumed that the probability was at least lower than the current probability.

How much more likely has the melt event become in the current climate, compared to the pre-industrial climate, based on observational data and model simulations?

When considering both climate simulations and observations, it becomes apparent that the probability of a Summit melt event, considering all months of the year, is 20 times higher in the current climate than in the pre-industrial climate. This shift in probability is statistically significant, indicating that melt extremes at the Summit in Greenland have become more likely due to human-induced climate change.

In contrast, for melt events in September, the probability of a melt event is not significantly higher in the current climate compared to the pre-industrial climate. While the likelihood of a Summit melt event in September is 15 times higher in the current climate, this change is not statistically significant, due to the lack of data. It is expected that as more data becomes available, a conclusive statement regarding melt events in the month of September can be made as well.

How will the rarity of the melt event change throughout the coming century, based on model simulations of future climate?

Adjacent to the attribution analysis, the analysis of future events holds significance. CESM HR model simulations, following the RCP8.5 emissions scenario, reveal a subtle rise in the likelihood of September melt events until 2040, beyond which a distinct upward trajectory emerges. A parallel progression emerges concerning melt events during other months of the year. Notably, an augmented probability is evident between 2000 and 2035, followed by a substantial surge from that point onward. The model simulations portray an escalating occurrence of melt events in the forthcoming years. This projection aligns with other studies forecasting temperature increases and increased melt phenomena at the Greenland Ice Sheet.

How much more likely will the melt event become by the end of the 21st century, compared to pre-industrial climate, based on model simulations?

Toward the end of this century, it is projected that Summit melt events in September will occur 570 times more frequently than they did in the pre-industrial period. Specifically, the probability of a September melt event is estimated at 46% for the period spanning 2070 to 2100. While the shift in the likelihood of a September melt event at the Summit is considered statistically significant, it's essential to exercise caution when interpreting the extent of this increase due to the substantial uncertainties inherent in the individual model probability ratios.

In line with this, the probability of experiencing melt events in any month of the year at the Summit reaches 83% by the end of this century, marking a 104-fold increase compared to the pre-industrial period. This substantial rise in likelihood is due to human-induced climate change and carries serious unfavorable implications. A heightened occurrence of melt events can result in increased mass loss, contributing to rising sea levels and, consequently, adversely impacting society.

To what extent can the September 2022 Extreme Melt Event at the Summit of Greenland be attributed to anthropogenic climate change and how will the likelihood of such an extreme melt event at the Summit in September change throughout the 21st century?

In summary, while the September 2022 melt event itself cannot be definitively attributed to climate change, there is evidence linking a 20-fold rise in melt events during other months to human-induced climate change. It is expected that when more data is available, a conclusive statement on September can be made as well. It's important to note that these conclusions rely on limited observations and climate models, introducing a degree of uncertainty. Specifically, the probability of September melt events in both the pre-industrial and current periods is uncertain due to the absence of known melt events.

The upward trend in melt events is expected to persist in the future, potentially increasing by up to 46% in September and 83% in any month by the end of this century. However, the precise quantity of this increase remains uncertain due to the limited amount of climate models considered.

An increase in extreme melt events can have far-reaching impacts on the Greenland Ice Sheet, leading to greater mass loss due to surface melting and runoff. The increased runoff from the Greenland Ice Sheet, in turn, has a direct influence on global sea levels, affecting coastal regions worldwide. These findings contribute to the understanding of extreme melt events. This could be of importance for the development of climate mitigation and adaptation strategies, much needed for the future.

7.2. Recommendations

This section outlines recommendations for improving the methodology used in this study and suggests directions for future research.

It is advisable for future attribution studies to consider selecting a variable of interest that exhibits a continuous range of values and avoids binary behaviour. Utilizing such variables would allow for the application of the method outlined in the research of Philip et al. (2020), which is more robust than the simplified method applied in this research.

To enhance the robustness of future studies, it is recommended to include additional climate model simulations from various models. This diversity in model simulations would provide a more comprehensive perspective on the climate system's response to the examined events and would reduce the uncertainty. It is also recommended to include models with a daily temporal resolution, as this would enable the consideration of Atmospheric River circumstances, further fortifying the robustness of future studies.

In order to attain a more holistic understanding of future climate scenarios, it is essential to consider multiple scenarios next to the one scenario considered in this study. Incorporating various scenarios will enable a more nuanced evaluation of potential outcomes, contributing to a more complete picture of the future climate of Greenland.

A promising avenue for further research could focus on investigating the atmospheric river circumstances associated with Summit melt events more. This aspect remains relatively unexplored in this study. However, understanding the driving factors behind melt events is as important as examining the melt events itself.

While attribution studies provide valuable insights, they are not exhaustive. Therefore, considering conducting a broader study encompassing extreme melt events could be a path of further research. This expanded perspective would offer a more holistic view of the extreme melt events on Greenland and their implications for the future climate.

Bibliography

Alley, R. B. (2000). *The Two-Mile Time Machine: Ice Cores, Abrupt Climate Change, and Our Future - Updated Edition*. Princeton University Press, rev - revised edition.

Alley, R. B. and Anandakrishnan, S. (1995). Variations in melt-layer frequency in the gisp2 ice core: implications for holocene summer temperatures in central greenland. *Annals of Glaciology*, 21.

AMAP (2021). Amap arctic climate change update 2021: Key trends and impacts. Tromso, Norway. viii+148pp.

Arias, P. A., Bellouin, N., Coppola, E., Jones, R. G., Krinner, G., Marotzke, J., Naik, V., Palmer, M. D., Plattner, G.-K., Rogelj, J., Rojas, M., Sillmann, J., Storelvmo, T., Thorne, P. W., Trewin, B., Rao, K. A., Adhikary, B., Allan, R. P., Armour, K., Bala, G., Barimalala, R., Berger, S., Canadell, J. G., Cassou, C., Cherchi, A., Collins, W., Collins, W. D., Connors, S. L., Corti, S., Cruz, F., Dentener, F. J., Dereczynski, C., Luca, A. D., Niang, A. D., Doblas-Reyes, F. J., Dosio, A., Douville, H., Engelbrecht, F., Eyring, V., Fischer, E., Forster, P., Fox-Kemper, B., Fuglestvedt, J. S., Fyfe, J. C., Gillett, N. P., Goldfarb, L., Gorodetskaya, I., Gutierrez, J. M., Hamdi, R., Hawkins, E., Hewitt, H. T., Hope, P., Islam, A. S., Jones, C., Kaufman, D. S., Kopp, R. E., Kosaka, Y., Kossin, J., Krakovska, S., Lee, J.-Y., Li, J., Mauritsen, T., Maycock, T. K., Meinshausen, M., Min, S.-K., Monteiro, P. M. S., Ngo-Duc, T., Otto, F., Pinto, I., Pirani, A., Raghavan, K., Ranasinghe, R., Ruane, A. C., Ruiz, L., Sallée, J.-B., Samset, B. H., Sathyendranath, S., Seneviratne, S. I., S"orensson, A. A., Szopa, S., Takayabu, I., Tréguier, A.-M., van den Hurk, B., Vautard, R., von Schuckmann, K., Zaehle, S., Zhang, X., and Zickfeld, K. (2021). Technical summary. In of Working Group I. to the Sixth Assessment Report of the Intergovernmental Panel on Climate Change [Masson-Delmotte, C., V., P. Z., Pirani, A., Connors, S. L., Péan, C., Berger, S., Caud, N., Chen, Y., Goldfarb, L., Gomis, M. I., Huang, M., Leitzell, K., Lonnoy, E., Matthews, J. B. R., Maycock, T. K., Waterfield, T., Yelekçi, O., Yu, R., and Zhou, B., editors, *Climate Change 2021: The Physical Science Basis*. Cambridge University Press, Cambridge, United Kingdom and New York, NY, USA, pp. 33−144.

Ballinger, T. J., Mote, T. L., Mattingly, K., Bliss, A. C., Hanna, E., van As, D., Prieto, M., Gharehchahi, S., Fettweis, X., Noël, B., Smeets, P. C., Reijmer, C. H., Ribergaard, M. H., and Cappelen, J. (2019). Greenland ice sheet late-season melt: Investigating multiscale drivers of k-transect events. *Cryosphere*, 13.

Beckmann, J. and Winkelmann, R. (2023). Effects of extreme melt events on ice flow and sea level rise of the greenland ice sheet. *The Cryosphere*, 17:3083–3099.

Bevis, M., Harig, C., Khan, S. A., Brown, A., Simons, F. J., Willis, M., Fettweis, X., van den Broeke, M. R., Madsen, F. B., Kendrick, E., Caccamise, D. J., van Dam, T., Knudsen, P., and Nylen, T. (2019). Accelerating changes in ice mass within greenland, and the ice sheet's sensitivity to atmospheric forcing. *Proceedings of the National Academy of Sciences of the United States of America*, 116.

Box, J. E., Wehrlé, A., van As, D., Kjeldsen, K. K., Ahlstrøm, A. P., and Picard, G. (2022). Greenland ice sheet rainfall, heat and albedo feedback impacts from the mid-august 2021 atmospheric river. *Geophysical Research Letters*.

Clausen, H., Gundestrup, N., Johnsen, S., Bindschadler, R., and Zwally, J. (1988). Glaciological investigations in the crête area, central greenland: A search for a new deep-drilling site. *Annals of Glaciology*, 10.

Collins, M., Knutti, R., Arblaster, J., Dufresne, J.-L., Fichefet, T., Friedlingstein, P., Gao, X., Gutowski, W., Johns, T., Krinner, G., Shongwe, M., Tebaldi, C., Weaver, A., Wehner, M., Allen, M., Andrews, T., Beyerle, U., Bitz, C., Bony, S., and Booth, B. (2013). *Long-term Climate Change: Projections, Commitments and Irreversibility*, pages 1029–1136. Intergovernmental Panel on Climate Change. Cambridge University Press, United Kingdom.

ECMWF (2023). Climate reanalysis. https://www.ecmwf.int/en/research/climate-reanalysis. [Online; accessed 2023-05-27].

Espinoza, V., Waliser, D. E., Guan, B., Lavers, D. A., and Ralph, F. M. (2018). Global analysis of climate change projection effects on atmospheric rivers. *Geophysical Research Letters*, 45.

Fettweis, X., Tedesco, M., van den Broeke, M., and Ettema, J. (2011). Melting trends over the greenland ice sheet (1958-2009) from spaceborne microwave data and regional climate models. *Cryosphere*, 5.

Guan, B. and Waliser, D. E. (2017). Atmospheric rivers in 20 year weather and climate simulations: A multimodel, global evaluation. *Journal of Geophysical Research*, 122.

Hanna, E., Cappelen, J., Fettweis, X., Mernild, S. H., Mote, T. L., Mottram, R., Steffen, K., Ballinger, T. J., and Hall, R. J. (2021). Greenland surface air temperature changes from 1981 to 2019 and implications for ice-sheet melt and mass-balance change. *International Journal of Climatology*, 41.

Hanna, E., Fettweis, X., Mernild, S. H., Cappelen, J., Ribergaard, M. H., Shuman, C. A., Steffen, K., Wood, L., and Mote, T. L. (2014). Atmospheric and oceanic climate forcing of the exceptional greenland ice sheet surface melt in summer 2012. *International Journal of Climatology*, 34.

Hofer, S., Tedstone, A. J., Fettweis, X., and Bamber, J. L. (2017). Decreasing cloud cover drives the recent mass loss on the greenland ice sheet. *Science Advances*, 3.

Huang, X., Swain, D. L., Walton, D. B., Stevenson, S., and Hall, A. D. (2020). Simulating and evaluating atmospheric river-induced precipitation extremes along the u.s. pacific coast: Case studies from 1980–2017. *Journal of Geophysical Research: Atmospheres*, 125.

iHESP (2023). Datasets. https://ihesp.github.io/ihesp_web/products/ihesp-products/Datasets.html#overview. [Online; accessed 2023-03-30].

IMAU, Institute for Marine and Atmospheric Research (2023). Ice and climate: Polar climate modelling. regional atmospheric climate model (racmo2). https://www.projects.science.uu.nl/iceclimate/models/racmo-model.php. [Online; accessed 2023-06-21].

Kay, J. E., Deser, C., Phillips, A., Mai, A., Hannay, C., Strand, G., Arblaster, J. M., Bates, S. C., Danabasoglu, G., Edwards, J., Holland, M., Kushner, P., Lamarque, J. F., Lawrence, D., Lindsay, K., Middleton, A., Munoz, E., Neale, R., Oleson, K., Polvani, L., and Vertenstein, M. (2015). The community earth system model (cesm) large ensemble project : A community resource for studying climate change in the presence of internal climate variability. *Bulletin of the American Meteorological Society*, 96.

Keegan, K. M., Albert, M. R., McConnell, J. R., and Baker, I. (2014). Climate change and forest fires synergistically drive widespread melt events of the greenland ice sheet. *Proceedings of the National Academy of Sciences of the United States of America*, 111:7964–7967.

Kim, T.-J., Kim, J., Park, C., Son, S.-W., Kim, J.-U., Kwon, S.-H., Moon, H., and Byun, Y.-H. (2023). Evaluation of a cmip6 multi-gcm ensemble for atmospheric rivers and precipitation over east asia. *Asia-Pacific Journal of Atmospheric Sciences*.

Lavers, D. A., Allan, R. P., Villarini, G., Lloyd-Hughes, B., Brayshaw, D. J., and Wade, A. J. (2013). Future changes in atmospheric rivers and their implications for winter flooding in britain. *Environmental Research Letters*, 8.

Lindsey, R. (2022). Unusually large, late melt spike on greenland in september 2022. https://www.climate.gov/news-features/event-tracker/unusually-large-late-melt-spike-greenland-september-2022. [Online; accessed 2023-05-24].

Liu, X., Chang, P., Fu, D., Saravanan, R., Wang, H., Rosenbloom, N., Zhang, S., and Wu, L. (2022). Improved simulations of atmospheric river climatology and variability in high□resolution cesm. *Journal of Advances in Modeling Earth Systems*, 14.

Mankoff, K., Fettweis, X., Solgaard, A., Langen, P., Stendel, M., Noël, B., van den Broeke, M. R., Karlsson, N., Box, J. E., and Kjeldsen, K. (2021). Greenland ice sheet mass balance from 1840 through next week. https://doi.org/10.22008/FK2/OHI23Z.

Mattingly, K. S., Mote, T. L., and Fettweis, X. (2018). Atmospheric river impacts on greenland ice sheet surface mass balance. *Journal of Geophysical Research: Atmospheres*, 123.

Meese, D. A., Gow, A. J., Grootes, P., Mayewski, P. A., Ram, M., Stuiver, M., Taylor, K. C., Waddington, E. D., and Zielinski, G. A. (1994). The accumulation record from the gisp2 core as an indicator of climate change throughout the holocene. *Science*, 266.

Messori, G., Woods, C., and Caballero, R. (2018). On the drivers of wintertime temperature extremes in the high arctic. *Journal of Climate*, 31.

Moon, T. A., Mankoff, K. D., Fausto, R. S., Fettweis, X., Loomis, B. D., Mote, T. L., Poinar, K., Tedesco, M., Wehrlé, A., and Jensen, C. D. (2022). Arctic report card 2022: Greenland ice sheet. *NOAA technical report OAR ARC*.

Moon, T. A., Tedesco, M., Box, J. E., Cappelen, J., Fausto, R. S., Fettweis, X., Korsgaard, N. J., Loomis, B. D., Mankoff, K. D., Mote, T. L., Wehrlé, A., and Ø A Winton (2021). Arctic report card 2021: Greenland ice sheet. *NOAA technical report OAR ARC*.

Moore, G. W. (2016). The december 2015 north pole warming event and the increasing occurrence of such events. *Scientific Reports*, 6.

Morlighem, M., Williams, C. N., Rignot, E., An, L., Arndt, J. E., Bamber, J. L., Catania, G., Chauché, N., Dowdeswell, J. A., Dorschel, B., Fenty, I., Hogan, K., Howat, I., Hubbard, A., Jakobsson, M., Jordan, T. M., Kjeldsen, K. K., Millan, R., Mayer, L., Mouginot, J., Noël, B. P., O'Cofaigh, C., Palmer, S., Rysgaard, S., Seroussi, H., Siegert, M. J., Slabon, P., Straneo, F., van den Broeke, M. R., Weinrebe, W., Wood, M., and Zinglersen, K. B. (2017). Bedmachine v3: Complete bed topography and ocean bathymetry mapping of greenland from multibeam echo sounding combined with mass conservation. *Geophysical Research Letters*, 44.

Mote, T. L. (2014). Measures greenland surface melt daily 25km ease-grid 2.0, version 1. https://nsidc.org/data/NSIDC-0533/versions/1.

NCAR (2023). Community earth system model. https://www.cesm.ucar.edu/. [Online; accessed 2023-03-30].

Neff, W. (2018). Atmospheric rivers melt greenland. *Nature Climate Change*, 8.

Nghiem, S. V., Hall, D. K., Mote, T. L., Tedesco, M., Albert, M. R., Keegan, K., Shuman, C. A., Digirolamo, N. E., and Neumann, G. (2012). The extreme melt across the greenland ice sheet in 2012. *Geophysical Research Letters*, 39.

Noël, B., van de Berg, W., van Wessem, J., van Meijgaard, E., van As, D., Lenaerts, J., Lhermitte, S., Kuipers Munneke, P., Smeets, C., van Ulft, L., van de Wal, R., and van den Broeke, M. (2018). Modelling the climate and surface mass balance of polar ice sheets using racmo2 - part 1: Greenland (1958-2016). *Cryosphere*, 12.

Noël, B., van Kampenhout, L., Lenaerts, J. T., van de Berg, W. J., and van den Broeke, M. R. (2021). A 21st century warming threshold for sustained greenland ice sheet mass loss. *Geophysical Research Letters*, 48.

NSF, National Science Foundation Office of Polar Programs (2023). Noaa esrl global monitoring laboratory. summit, greenland [sum]. https://gml.noaa.gov/dv/site/?stacode=SUM. [Online; accessed 2023-07-13].

NSF, Summit Station Science Coordination Office (2023). Summit station. https://geo-summit.org/summit-station. [Online; accessed 2023-06-08].

NSIDC (2019a). Large ice loss on the greenland ice sheet in 2019. http://nsidc.org/greenland-today/2019/11/large-ice-loss-on-the-greenland-ice-sheet-in-2019/. [Online; accessed 2022-10-25].

NSIDC (2019b). A record melt event in mid-june 2019. http://nsidc.org/greenland-today/2019/07/a-record-melt-event-in-mid-june/. [Online; accessed 2022-09-07].

NSIDC (2022). A melt spike in september? https://nsidc.org/greenland-today/2022/09/a-melt-spike-in-september/. [Online; accessed 2022-09-27].

Oppenheimer, M., Glavovic, B., Hinkel, J., van de Wal, R., Magnan, A., Abd-Elgawad, A., Cai, R., Cifuentes-Jara, M., DeConto, R., Ghosh, T., Hay, J., Isla, F., Marzeion, B., Meyssignac, B., and Sebesvari, Z. (2019). Sea level rise and implications for low-lying islands, coasts and communities. *In: IPCC Special Report on the Ocean and Cryosphere in a Changing Climate*, pages 321–445.

Patel, K. and Mooney, C. (2022). For first time on record, greenland saw extensive melting in september. https://www.washingtonpost.com/climate-environment/2022/09/06/greenland-ice-melt-heat-wave-summer/. [Online; accessed 2023-05-24].

Payne, A. E. and Magnusdottir, G. (2015). An evaluation of atmospheric rivers over the north pacific in cmip5 and their response to warming under rcp 8.5. *Journal of Geophysical Research: Atmospheres*, 120.

Philip, S., Kew, S., van Oldenborgh, G. J., Otto, F., Vautard, R., van der Wiel, K., King, A., Lott, F., Arrighi, J., Singh, R., and van Aalst, M. (2020). A protocol for probabilistic extreme event attribution analyses. *Advances in Statistical Climatology, Meteorology and Oceanography*, 6.

Picard, G. (2022). Surface melt on the antarctic and greenland ice sheets (1979 - 2021). https://snow.univ-grenoble-alpes.fr/melting/. [Online; accessed 2023-05-05].

Picard, G. (2023). Near real-time surface melt in greenland. https://snow.univ-grenoble-alpes.fr/melting/nrt-greenland/. [Online; accessed 2023-05-05].

Picard, G. and Fily, M. (2006). Surface melting observations in antarctica by microwave radiometers: Correcting 26-year time series from changes in acquisition hours. *Remote Sensing of Environment*, 104.

Rae, J. G., Aoalgeirsdóttir, G., Edwards, T. L., Fettweis, X., Gregory, J. M., Hewitt, H. T., Lowe, J. A., Lucas-Picher, P., Mottram, R. H., Payne, A. J., Ridley, J. K., Shannon, S. R., van De Berg, W. J., van de Wal, R. S., and van den Broeke, M. R. (2012). Greenland ice sheet surface mass balance: Evaluating simulations and making projections with regional climate models. *Cryosphere*, 6.

Ramos, A. M., Tomé, R., Trigo, R. M., Liberato, M. L., and Pinto, J. G. (2016). Projected changes in atmospheric rivers affecting europe in cmip5 models. *Geophysical Research Letters*, 43.

Sasgen, I., Wouters, B., Gardner, A. S., King, M. D., Tedesco, M., Landerer, F. W., Dahle, C., Save, H., and Fettweis, X. (2020). Return to rapid ice loss in greenland and record loss in 2019 detected by the grace-fo satellites. *Communications Earth & Environment*.

Schwalm, C. R., Glendon, S., and Duffy, P. B. (2020). Rcp8.5 tracks cumulative co2 emissions. *Proceedings of the National Academy of Sciences*, 117(33):19656–19657.

Small, R. J., Bacmeister, J., Bailey, D., Baker, A., Bishop, S., Bryan, F., Caron, J., Dennis, J., Gent, P., Hsu, H. M., Jochum, M., Lawrence, D., Muñoz, E., Dinezio, P., Scheitlin, T., Tomas, R., Tribbia, J., Tseng, Y. H., and Vertenstein, M. (2014). A new synoptic scale resolving global climate simulation using the community earth system model. *Journal of Advances in Modeling Earth Systems*, 6.

Steffen, K., Houtz, D., Vandecrux, B., Abdalati, W., Bayou, N., Box, J., Colgan, W., Pernas, L. E., Griessinger, N., Haas-Artho, D., Heilig, A., Hubert, A., Enescu, I. I., Johnson-Amin, N., Karlsson, N. B., Kurup, R., McGrath, D., Naderpour, R., Østerby Pederson, A., Perren, B., Phillips, T., Plattner, G.-K., Proksch, M., Revheim, M. K., Saettele, M., Schneebeli, M., Sampson, K., Starkweather, S., Steffen, S., Stroeve, J., Walter, B., Øyvind Andreas Winton, and Zwally, J. (2020). Greenland climate network (gc-net) data. https://www.envidat.ch/dataset/gcnet.

Tedesco, M. and Fettweis, X. (2020). Unprecedented atmospheric conditions (1948-2019) drive the 2019 exceptional melting season over the greenland ice sheet. *Cryosphere*, 14.

Tedesco, M., Fettweis, X., Mote, T., Wahr, J., Alexander, P., Box, J. E., and Wouters, B. (2013). Evidence and analysis of 2012 greenland records from spaceborne observations, a regional climate model and reanalysis data. *Cryosphere*, 7:615–630.

Trusel, L. D., Das, S. B., Osman, M. B., Evans, M. J., Smith, B. E., Fettweis, X., McConnell, J. R., Noël, B. P., and van den Broeke, M. R. (2018). Nonlinear rise in greenland runoff in response to post-industrial arctic warming. *Nature*, 564.

ULiège and Fettweis, X. (2023). Real-time state of the 2022-2023 greenland ice sheet surface mass balance as simulated by the regional climate model mar. `https://www.climato.uliege.be/cms/c_5652668/fr/climato-greenland`. [Online; accessed 2023-07-10].

van der Wiel, K. and Bintanja, R. (2021). Contribution of climatic changes in mean and variability to monthly temperature and precipitation extremes. *Communications Earth and Environment*, 2.

Vandecrux, B., Box, J. E., Ahlstrøm, A. P., Andersen, S. B., Bayou, N., Colgan, W. T., Cullen, N. J., Fausto, R. S., Haas-Artho, D., Heilig, A., Houtz, D. A., How, P., Enescu, I. I., Karlsson, N. B., Buchholz, R. K., Mankoff, K. D., Mcgrath, D., Molotch, N. P., Perren, B., Revheim, M. K., Rutishauser, A., Sampson, K., Schneebeli, M., Starkweather, S., Steffen, S., Weber, J., Wright, P. J., Zwally, H. J., and Steffen, K. (2023). The historical greenland climate network (gc-net) curated and augmented level 1 dataset. *Earth Syst. Sci. Data Discuss. [preprint]*. In review.

Vihma, T. (2017). *Weather Extremes Linked to Interaction of the Arctic and Midlatitudes*, volume 226, chapter 2. The American Geophysical Union.

WWA (2016). Unusually high temperatures at the north pole, winter 2016. `https://www.worldweatherattribution.org/north-pole-nov-dec-2016/`. [Online; accessed 2022-09-07].

Zhang, P., Chen, G., Ma, W., Ming, Y., and Wu, Z. (2021). Robust atmospheric river response to global warming in idealized and comprehensive climate models. *Journal of Climate*, 34.

Zhao, M. (2020). Simulations of atmospheric rivers, their variability, and response to global warming using gfdl's new high-resolution general circulation model. *Journal of Climate*, 33.

Appendices

A

Additional Figures

A.1. September mean Temperature and Specific Humidity

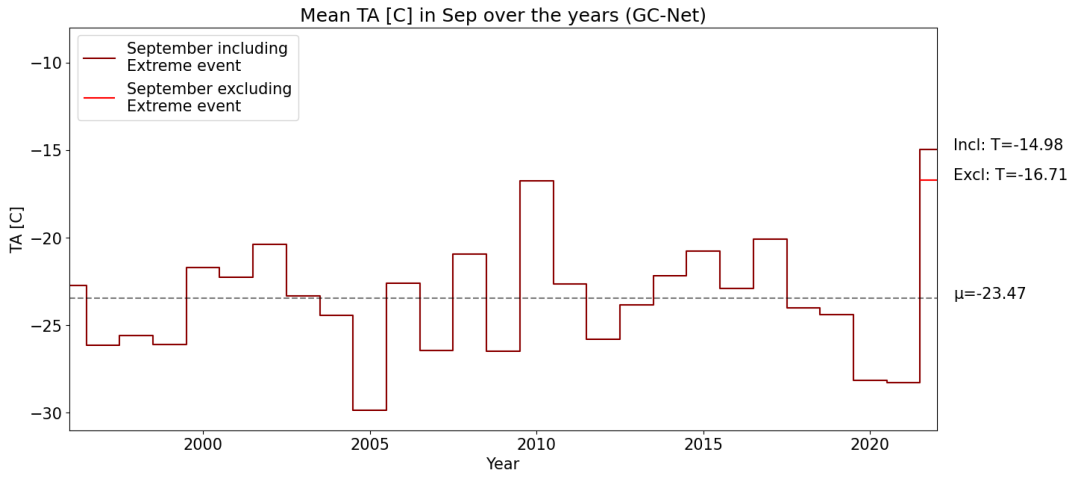

Figure A.1: Mean temperature [°C] in September over the years, based on the GC-Net station data. In September 2022 the mean temperature is -14.98°C, when the melt event of 3-6 September is excluded from the mean, the value lowers to -16.71°C.

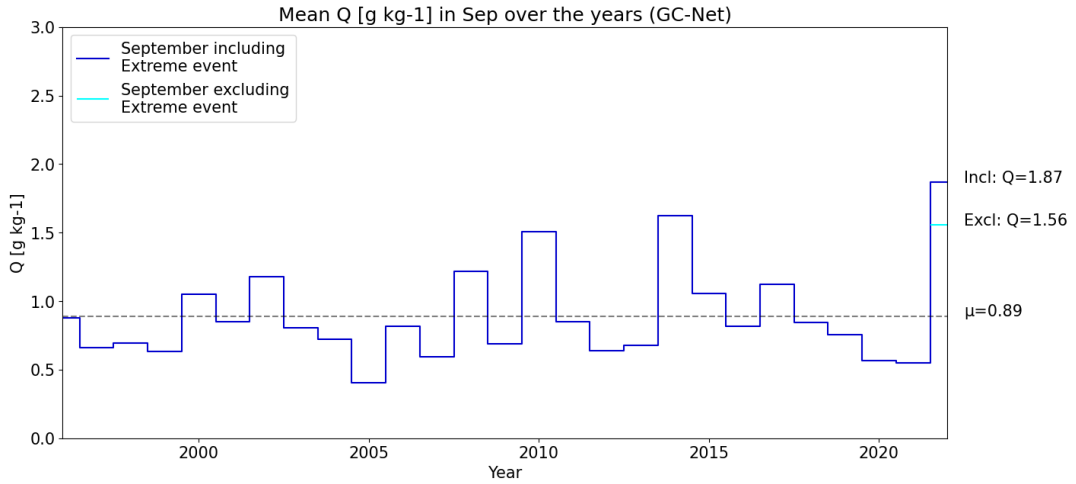

Figure A.2: Mean specific humidity [g/kg] in September over the years, based on the GC-Net station data. In September 2022 the mean humidity is 1.87 g/kg, when the melt event of 3-6 September is excluded from the mean, the value lowers to 1.56 g/kg.

A.2. Melt maps RACMO

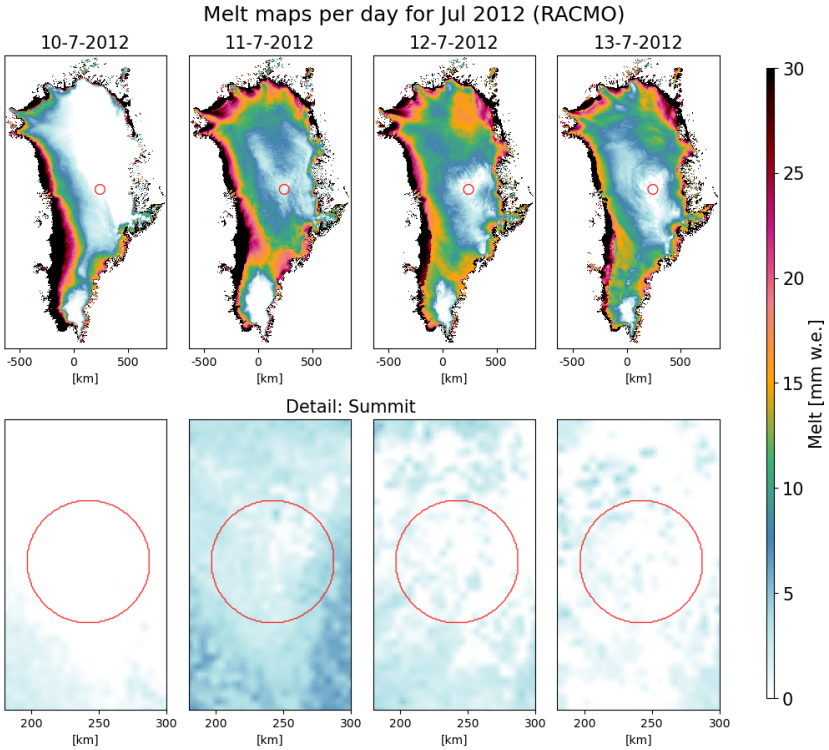

Figure A.3: Melt maps per day for 10-13 Jul 2012 (RACMO)

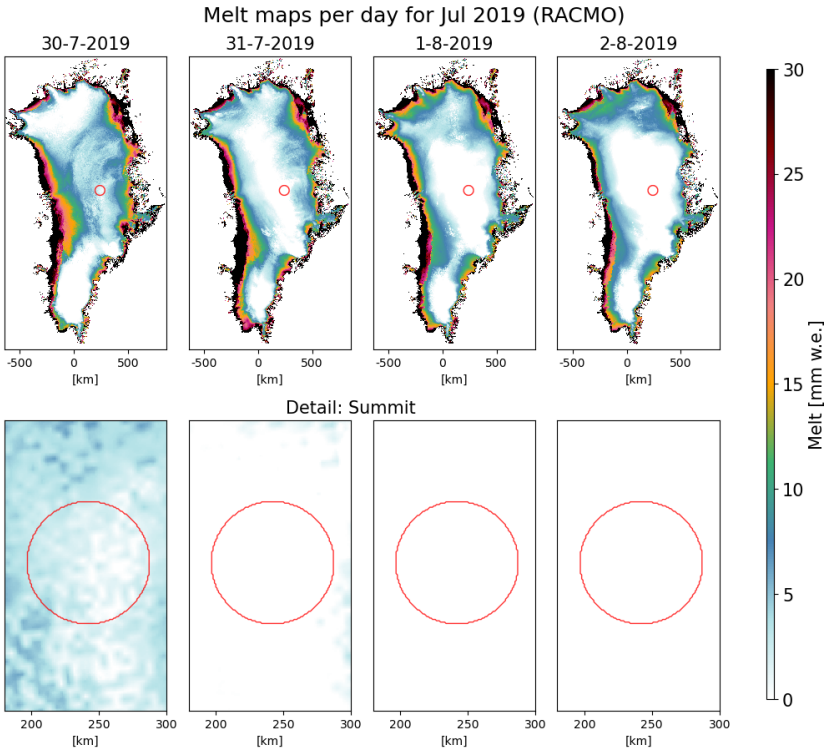

Figure A.4: Melt maps per day for 30 July - 2 August 2019 (RACMO)

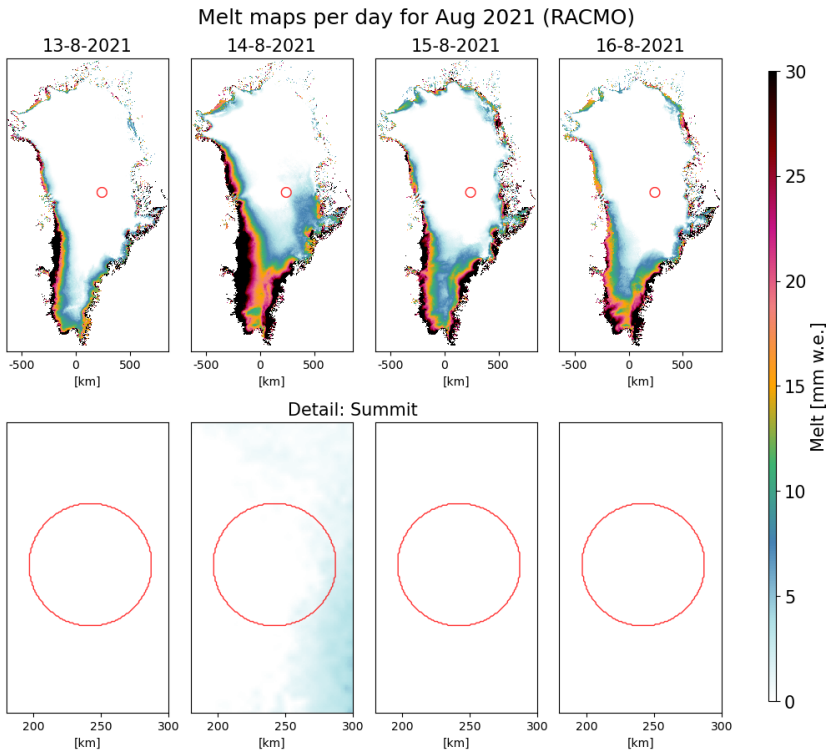

Figure A.5: Melt maps per day for 13-16 Aug 2021 (RACMO)

A.3. Melt maps MAR

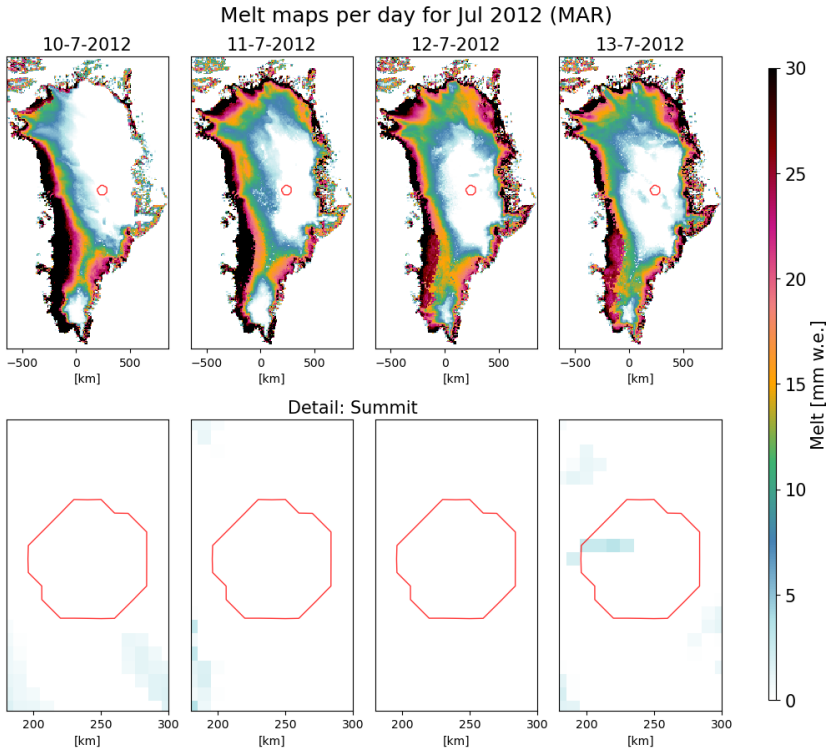

Figure A.6: Melt maps per day for 10-13 Jul 2012 (MAR)

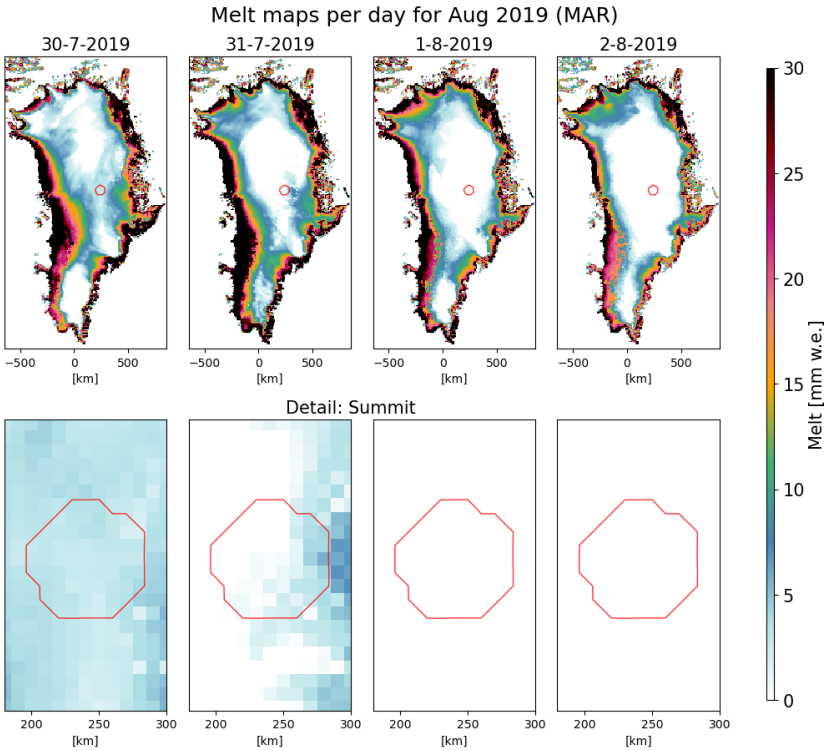

Figure A.7: Melt maps per day for 30 July - 2 August 2019 (MAR)

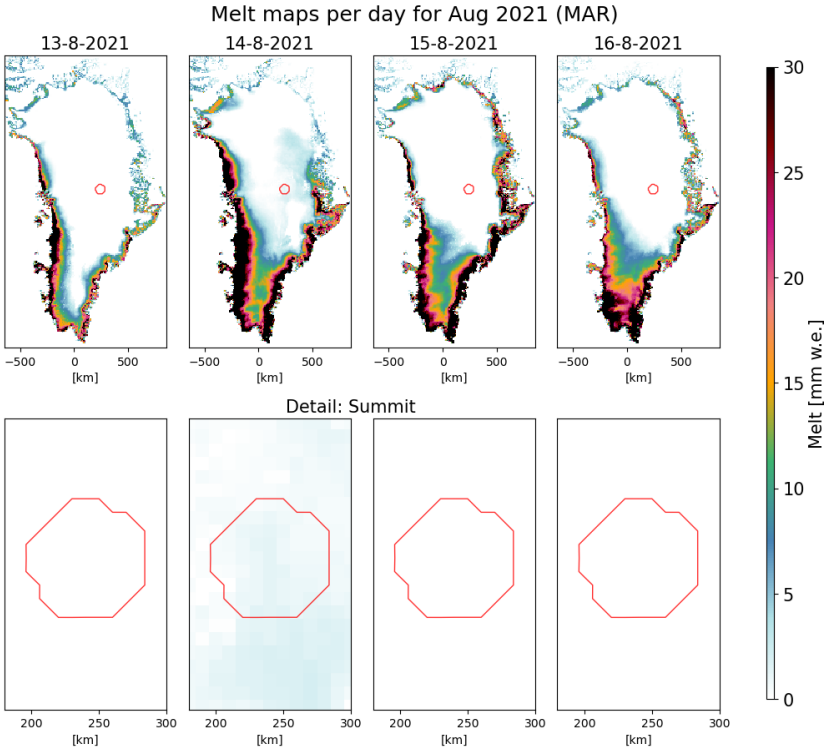

Figure A.8: Melt maps per day for 13-16 Aug 2021 (MAR)

A.4. Melt record multiple thresholds per data source

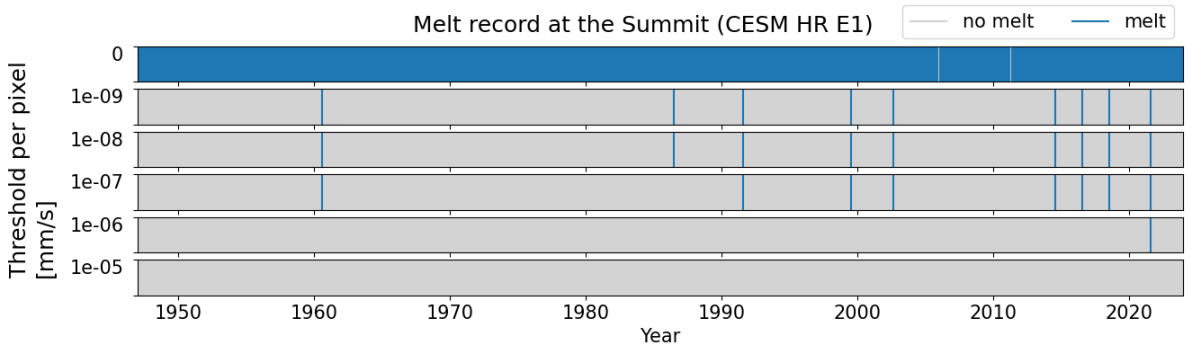

Figure A.9: Melt record at the Summit (CESM HR E1) multiple thresholds

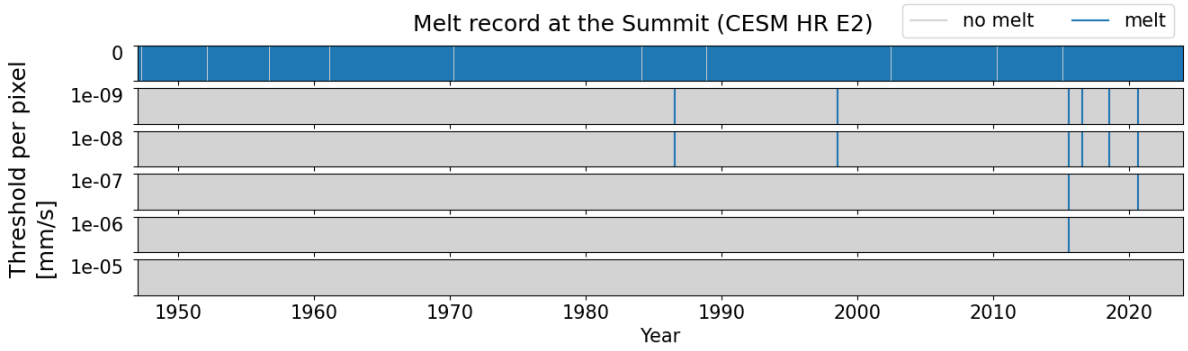

Figure A.10: Melt record at the Summit (CESM HR E2) multiple thresholds

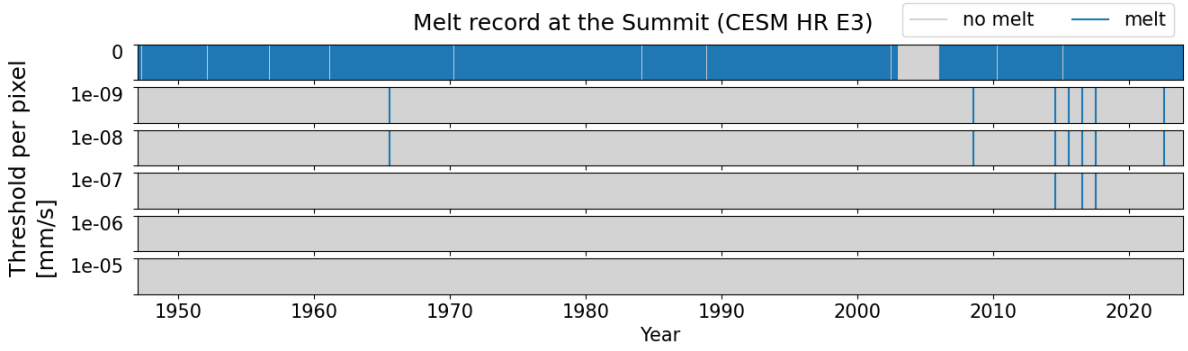

Figure A.11: Melt record at the Summit (CESM HR E3) multiple thresholds

B

Additional Tables

B.1. Results - Comparison Atmospheric River events and Melt events

In the tables in this section, table B.1 to B.4, the first four rows represent the number of days with Melt, AR, both or none. The last three rows present metrics that indicate how well the Melt and AR events agree. The last row is the harmonic mean of the two rows above it, summarizing the percentages into one value.

Days with	GC-Net station	PM	RACMO	MAR
Melt and AR	4	11	10	4
Melt, no AR	6	6	0	2
AR, no Melt	23	16	17	23
No Melt, no AR	9611	14716	23349	26269
% days with Melt that also have AR	40.00%	64.71%	100.00%	66.67%
% days with AR that also have melt	14.81%	40.74%	37.04%	14.81%
Harmonic mean	21.62%	50.00%	54.05%	24.24%

Table B.1: Results comparison AR events and Melt events in observational data.

Months with	Historical		
	E1	E2	E3
Melt and AR	6	4	6
Melt, no AR	1	1	0
AR, no Melt	136	96	89
No Melt, no AR	1906	1089	1061
% months with Melt that also have AR	85.71%	80.00%	100.00%
% months with AR that also have melt	4.23%	4.00%	6.32%
Harmonic mean	8.05%	7.62%	11.88%

Table B.2: Results comparison AR events and Melt events in climate model data for the Historical period (1850/1920-2020).

Months with	Future		
	E1	E2	E3
Melt and AR	42	65	62
Melt, no AR	18	1	0
AR, no Melt	145	135	141
No Melt, no AR	676	742	740
% months with Melt that also have AR	70.00%	98.48%	100.00%
% months with AR that also have melt	22.46%	32.50%	30.54%
Harmonic mean	34.01%	48.87%	46.79%

Table B.3: Results comparison AR events and Melt events in climate model data for the Future period (2021-2100).

Months with	Pre-Industrial
Melt and AR	4
Melt, no AR	0
AR, no Melt	347
No Melt, no AR	5636
% months with Melt that also have AR	100.00%
% months with AR that also have melt	1.14%
Harmonic mean	2.25%

Table B.4: Results comparison AR events and Melt events in climate model data for the Pre-Industrial period (500x 1850).

B.2. Results - Probabilities observations

September	Probability	95% CI	
		2.5%	97.5%
Ice core (K. (2014)) CTRL	0.0008	0.0000	0.0016
Ice core (K. (2014)) HIST	0.0008	0.0000	0.0016
PM	0.0008	0.0000	0.0016
RACMO	0.0008	0.0000	0.0016
MAR	0.0008	0.0000	0.0016
Ice cores mean CTRL	0.0008	0.0000	0.0016
Observations mean HIST	0.0008	0.0004	0.0012

Table B.5: Probabilities of observations for September for the Pre-Industrial and Current period with 95% Confidence Intervals (CI).

Any month	Probability	95% CI	
		2.5%	97.5%
Ice core (A. (1995)) CTRL	0.0065	0.0051	0.0080
Ice core (M. (1994)) CTRL	0.0053	0.0020	0.0094
Ice core (K. (2014)) CTRL	0.0067	0.0000	0.0200
Ice core (K. (2014)) HIST	0.0667	0.0000	0.1667
PM	0.1333	0.0333	0.2667
RACMO	0.1000	0.0000	0.2333
MAR	0.1667	0.0333	0.3000
Ice cores mean CTRL	0.0062	0.0036	0.0108
Observations mean HIST	0.1167	0.0653	0.1796

Table B.6: Probabilities of observations for Any month for the Pre-Industrial and Current period with 95% Confidence Intervals (CI).

B.3. Results - Probabilities climate models

September	Probability	95% CI	
		2.5%	97.5%
CESM HR CTRL	0.0008	0.0000	0.0016
CESM HR E1 HIST	0.0333	0.0000	0.1000
CESM HR E2 HIST	0.0333	0.0000	0.1000
CESM HR E3 HIST	0.0008	0.0000	0.0016
CESM HR E1 FUT	0.4667	0.3000	0.6333
CESM HR E2 FUT	0.4667	0.3000	0.6333
CESM HR E3 FUT	0.4333	0.2667	0.6000
CESM HR mean CTRL	0.0008	0.0000	0.0016
CESM HR mean HIST	0.0225	0.0068	0.0539
CESM HR mean FUT	0.4556	0.3593	0.5518

Table B.7: Probabilities of CESM HR for September with 95% Confidence Intervals (CI).

Any month	Probability	95% CI	
		2.5%	97.5%
CESM HR CTRL	0.0080	0.0020	0.0160
CESM HR E1 HIST	0.2000	0.0667	0.3667
CESM HR E2 HIST	0.1333	0.0333	0.2667
CESM HR E3 HIST	0.1667	0.0333	0.3000
CESM HR E1 FUT	0.8000	0.6333	0.9333
CESM HR E2 FUT	0.7667	0.6000	0.9000
CESM HR E3 FUT	0.9333	0.8333	1.0000
CESM HR mean CTRL	0.0080	0.0020	0.0160
CESM HR mean HIST	0.1667	0.0955	0.2505
CESM HR mean FUT	0.8333	0.7480	0.9000

Table B.8: Probabilities of CESM HR for Any month with 95% Confidence Intervals (CI).

B.4. Results - Mean probabilities

September	Probability	95% CI	
		2.5%	97.5%
All CTRL	0.0008	0.0002	0.0014
All HIST	0.0101	0.0034	0.0236
All FUT	0.4556	0.3593	0.5518

Table B.9: Mean probabilities of all observations and models together for September with 95% Confidence Intervals (CI).

Any month	Probability	95% CI	
		2.5%	97.5%
All CTRL	0.0066	0.0042	0.0107
All HIST	0.1381	0.0957	0.1889
All FUT	0.8333	0.7480	0.9000

Table B.10: Mean probabilities of all observations and models together for Any month with 95% Confidence Intervals (CI).

B.5. Results - Probability Ratios

September	Probability Ratio	95% CI 2.5%	95% CI 97.5%
PR pi-c Ice core	1.00	0.00	2.41
PR pi-c PM	1.00	0.00	2.41
PR pi-c RACMO	1.00	0.00	2.41
PR pi-c MAR	1.00	0.00	2.41
PR pi-c Observations	1.00	0.29	1.71
PR pi-c CESM HR E1	41.67	0.00	134.77
PR pi-c CESM HR E2	41.67	0.00	134.82
PR pi-c CESM HR E3	1.00	0.00	2.41
PR pi-c Models	28.11	0.33	72.00
PR pi-c Synthesis	14.56	0.66	36.50
PR pi-f CESM HR E1	583.33	0.00	1202.93
PR pi-f CESM HR E2	583.33	0.00	1202.77
PR pi-f CESM HR E3	541.67	0.00	1121.57
PR pi-f Models	569.44	219.16	919.64

Table B.11: Probability Ratios for September for the Pre-Industrial versus Current period (pi-c) and the Pre-Industrial versus Future period (pi-f) with 95% Confidence Intervals (CI).

Any month	Probability Ratio	95% CI 2.5%	95% CI 97.5%
PR pi-c Ice core	10.79	0.00	28.90
PR pi-c PM	21.58	3.14	48.61
PR pi-c RACMO	16.18	0.00	40.99
PR pi-c MAR	26.97	2.73	56.65
PR pi-c Observations	18.88	9.62	31.51
PR pi-c CESM HR E1	25.00	0.00	57.57
PR pi-c CESM HR E2	16.67	0.00	40.24
PR pi-c CESM HR E3	20.83	0.00	47.51
PR pi-c Models	20.83	8.08	36.92
PR pi-c Synthesis	19.86	11.98	30.08
PR pi-f CESM HR E1	100.00	22.17	201.53
PR pi-f CESM HR E2	95.83	21.01	193.26
PR pi-f CESM HR E3	116.67	28.29	233.76
PR pi-f Models	104.17	57.68	165.21

Table B.12: Probability Ratios for Any Month for the Pre-Industrial versus Current period (pi-c) and the Pre-Industrial versus Future period (pi-f) with 95% Confidence Intervals (CI).

C

Results by Data Source

This appendix presents an overview of the results of the melt event detection and probability computations. The results are presented per data source for the observational data and the climate model data. For the climate model data, the melt detection and probability computations are done for the historical climate, the pre-industrial climate and the future climate considering all months together as well as the month of September separately.

C.1. Ice Core results

Keegan et al. (2014) studied six ice cores from four sites, including Summit, to investigate widespread melt events in the period 1750-2012. They found that widespread melt, including melt at the Summit, occurred only in the summer period of 1889 and 2012, see figure C.1 for a schematization of the ice core. The widespread melt events were caused by a combination of unusually warm circumstances and a lowered albedo (Keegan et al., 2014). The lowered albedo was caused by black carbon deposits from forest fires or fossil fuel combustion.

Trusel et al. (2018) studied ice cores from central west Greenland to quantify annual melting between 1650 and 2015. The melt observed in the ice cores is compared to the modelled and observed melt across the ice sheet. A significant positive correlation is found between the ice core melt record and the RACMO2-modelled melt, as well as with the satellite-observed melt (Trusel et al., 2018). These ice core melt records reveal that the 2012 melt rates were exceptionally high for the past 350 years. This is in line with the results from Keegan et al. (2014).

These melt events did not occur in the time span of interest, namely September. However, they did occur in the region of interest, namely the Summit. The two events occurring over a period of 262 years, give an indication of the rarity of melt at the Summit. Therefore, the probability of a year with melt at the Summit between 1750 and 2012 is $p_{All} = 1/132.5$. The probability of a year with melt in September is approximately 0 because no events were detected in September $p_{Sep} =\rightarrow 0$. Since the date of the melt events is known, the probability of melt for the pre-industrial climate as well as the current climate can be computed. The probability for the pre-industrial climate is computed over the period 1750-1900 and is 1/150e. The probability for the current climate is computed over the most recent 30 years, between 1982-2012, and is 1/30e.

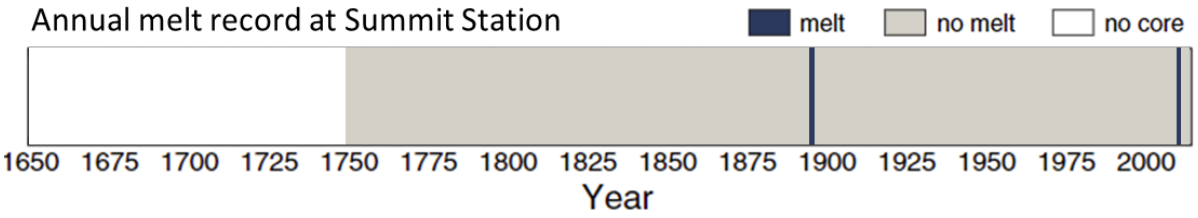

Figure C.1: Annual melt record at Summit Station. Melt in 1889 and 2012 at the Summit (visualisation of information in Keegan et al. (2014)).

Alley and Anandakrishnan (1995) studied the GISP2 ice core, it was drilled 28 km west of the Summit and contains more than 10.000 years of information. Melt is scarce in the GISP2 ice core, so the occurrence of melt in a year is recorded rather than the melt thickness. Results show that the melt frequency over the past 10.000 years averages once per 153 years. However large differences exist within this period. About 7000-8000 years before present (BP), the melt frequency at the Summit was at its peak and since then has decreased significantly. Between 5500-8500 years BP, a melt event occurred once every 82 years, whereas, between 1000-4000 years BP, a melt event occurred once every 250 years. These frequencies are 1.5 standard deviations above and two standard deviations below the mean respectively. A similar increase in frequency occurred between 9000-12000 BP and 5500-8500 BP. Alley and Anandakrishnan (1995) attribute this change to a decrease in summer temperatures of 1.3 $^\circ$ C.

Meese et al. (1994) studied the same ice core, the GISP2 ice core, over the Holocene. They found thin melt layers, showing that 8 melt events occurred in the past 1500 years. The most recent melt event (since 1994) was the 1889 melt event, the other seven melt events occurred between 500-1250. These findings are supported by Clausen et al. (1988). They studied eight shallow ice cores from the region around the Summit that covered the period 1622-1984. In all ice cores, a distinct melt layer was found in the 1889 annual layer. The eight melt events occurring in 1500 years, as found by Meese et al. (1994), lead to an average occurrence of one melt event per 187.5 years.

Data	**Period**	**Probability Sep**	**Probability All**	**Source**
Ice core	1750 - 2012	$\rightarrow 0$	1/132.5	Keegan et al. (2014)
	1750 - 1900	$\rightarrow 0$	1/150	
	1990 - 2012 (2020)	$\rightarrow 0$	1/22 (1/15)	
Ice core	10.000 BP - 1993	-	1/153	Alley and Anandakrishnan (1995)
	8.500 - 5.500 BP	-	1/82	
	4.000 - 1.000 BP	-	1/250	
Ice core	500 - 1993	-	1/187.5	Meese et al. (1994)

Table C.1: Probability of melt occurring at the Summit retrieved from Ice Core data

Due to the extensive time span of the ice core data, their results can be used to identify the probability of melt in the pre-industrial period. The probability determined from Keegan et al. (2014) for 1750-1900 is combined with the probability determined by Alley and Anandakrishnan (1995) for 10.000 BP - 1993 and by Meese et al. (1994) for 500 - 1993. The combination of these probabilities results in a probability representing the pre-industrial period of 1/163.5.

The ice core results of Keegan et al. (2014) can be used to determine a probability for the current climate as well. The ice core results cover the period 1990-2012 within the current period, results for 2012-2020 are non-existent. One event is detected for this time period, which results in a probability of 1/22. For a fair representation of the period 1990-2020, the choice is made to estimate the number of melt events for the missing period (2013-2020) and include them in the probability computation. Based on literature (Sasgen et al. (2020), NSIDC (2019b), Tedesco and Fettweis (2020)) it is estimated that if the ice core was retrieved after 2020, the melt event of 2019 would have been present in the ice core. Therefore one event is added to the ice core data before the probability is computed. This results in a probability value for the current climate of 1/15.

C.2. Station data: results event detection

The results from the event detection can be found here. The dates with temperatures above $-0.1°C$ are visualised in figure C.2 and displayed in table C.2 for the GC-Net station data and in table C.3 for the NOAA station data.

In the GC-Net dataset, 10 days with melt are detected, which can be clustered into six melt events. The melt events in mid-July 2012 and end-July/beginning of August 2019 both encompass three days in the GC-Net data. These melt events are known to be the largest melt events in the satellite-era (Nghiem et al. (2012), Tedesco et al. (2013), Sasgen et al. (2020), NSIDC (2019a)) and are no surprise to be found in the Summit Station data. The two melt events in August 2011 both consist of two hours of melt on one day, these melt events at the summit are not known from literature. The last two melt

events that are found occurred in mid-July 2021 and mid-August 2021. The event in mid-August is known to for the rain that fell for the first time at the summit (Box et al. (2022) Lindsey (2022)). The event in July 2021 is not known from earlier publications.

In the NOAA dataset, four days with melt are detected during three melt events. These are the mid July 2012, end of July 2019 and mid August 2021 events. These three events are present in the GC-Net Summit station data as well. On the 11th of July 2012 melt is detected for seven hours. On 30 and 31 July 2019 melt is detected for 11 and 6 hours respectively. This melt event is detected in both station datasets, however, in the NOAA data, melt is detected on the 31st of July 2019, where there is no melt detected in the GC-Net data. On the 14th of August 2021, 10 hours of melt are detected.

One should pay attention to the fact that the GC-Net station data spans the period 1997-2021 and that the NOAA station data only spans the period 2009-2021.

These findings are in line with Moon et al. (2021), who report three melt events between 1989-2020, in 1995, 2012 and 2019, based on measurements at GEOSummit station (NOAA dataset).

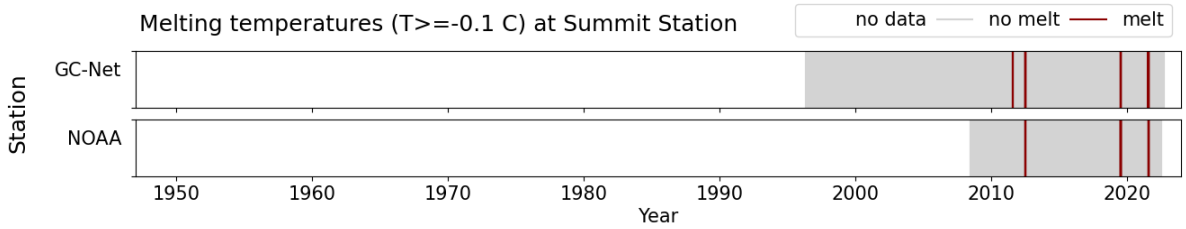

Figure C.2: Melting temperature (T>=-0.1 ° C) at GC-Net Summit Station and NOAA Summit Station

Event	Days	Year	Hours with T>0C
1	1 August	2011	2
2	8 August	2011	2
3	11, 12 & 16 July	2012	8, 2 & 1
4	30 July, 1 & 2 August	2019	6, 1 & 2
5	12 July	2021	1
6	14 August	2021	9

Table C.2: Dates with temperatures above -0.1 degree Celsius at Summit Station (GC-Net)

Event	Day	Year	Hours with T>0C
1	11 July	2012	7
2	30 & 31 July	2019	11 & 6
3	14 August	2021	10

Table C.3: Dates with temperatures above -0.1 degree Celsius at Summit Station (NOAA)

C.3. Passive Microwave results

The melt detection is applied to the Passive Microwave data. This results in the detection of six melt events in the period where observations are available (1980-2021). The melt events are visualised in C.3 and the dates of the melt events are listed in table C.4. Of the six detected melt events, two took place in June, three in July and one in August. No melt events are observed in September. Furthermore, it strikes that all melt events are detected for at least two days, up to a maximum of 5 days for the July 2012 event. In 2019 two melt events are detected.

From the detected melt events, the probability of melt in a year is computed. For the current climate/historical period, which is defined as 1990 - 2020, five events are detected in four unique years, when all months are considered. Four years with melt in a period of thirty years results in a probability of $p_{All} = 4/30 = 1/7.5$. In September no events were detected, which results in a probability approaching zero $p_{Sep} \to 0$. The probabilities are summarized in table C.5.

The Passive Microwave data spans a period of 41 years, therefore a time series of the probability can be computed. The time series of the Passive Microwave data is visualised in figure 5.5.

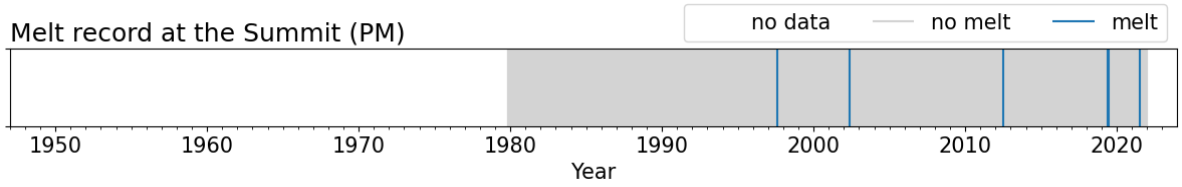

Figure C.3: Melt record at the Summit (PM)

Event	Days	Year
1	12 - 13 August	1997
2	28 June - 1 July	2002
3	10 - 14 July	2012
4	12 - 13 June	2019
5	30 - 31 July	2019
6	27 - 28 July	2021

Table C.4: Melt events in PM data

Data	Period	Probability Sep	Probability All
PM	1980-2021	$\rightarrow 0$	1/8.2
	1990-2020	$\rightarrow 0$	1/7.5

Table C.5: Probability of melt occurring at the Summit. Based on Passive Microwave observations.

C.4. Reanalysis forced RACMO results

In the RACMO data, a total of eight melt events between 1958 and 2021 have been identified, and the specific dates of these events can be found in table C.7, while a visual representation is provided in figure C.4.

Figure C.4 and table C.7 display that two events were detected in 2012 as well as in 2019. Furthermore, the duration of these events varied, ranging from single-day occurrences to multi-day events. During the period of analysis from 1990 to 2020, which serves as the basis for computing probabilities, five melt events were identified in three distinct years. Consequently, the probability of experiencing a "year with melt" is determined to be $p_{All} = 1/10$. It is noteworthy that none of these events took place in September, leading to an approaching zero probability of a year with melt in September, denoted as $p_{Sep} \rightarrow 0$.

To assess the temporal dynamics of melt probabilities based on the available ERA-forced RACMO data, a time series of these probabilities is generated. This time series can be observed in figure 5.5.

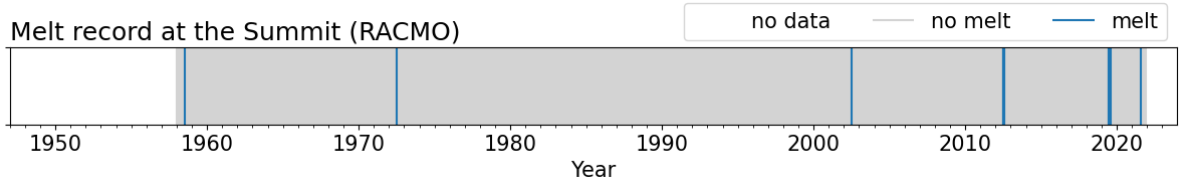

Figure C.4: Melt record at the Summit (RACMO) (threshold = 636 pixels with 0.8 mm w.e. melt)

Data	Period	Probability Sep	Probability All
RACMO	1958-2021	$\rightarrow 0$	1/10.5
	1990-2020	$\rightarrow 0$	1/10

Table C.6: Probability of melt occurring at the Summit. Based on ERA forced RACMO data.

Event	Days	Year
1	19 July	1958
2	5 July	1972
3	28 June	2002
4	11-13 July	2012
5	29-30 July	2012
6	12-13 June	2019
7	30 July	2019
8	14 August	2021

Table C.7: Melt events in ERA forced RACMO data (threshold = 636 pixels with 0.8 mm w.e. melt)

C.5. Reanalysis forced MAR results

For the MAR data, a threshold for a melt event to be detected is set to at least six pixels having at least 2.3 mm w.e. melt per day. This leads to ten melt events in ten years between 1950 - 2021, see table C.8 and figure C.5 for an overview of the events. Of the ten melt events, five events occurred between 1990-2020, this leads to a probability of a year with melt at the Summit of $p_{All} = 1/6$. In the MAR data, no melt in September is detected. This leads to a probability approaching zero for September $p_{Sep} \rightarrow 0$.

The MAR data spans a period of 71 years. For this period, the probability of melt in a year is computed for periods of 30 years with increments of 1 year to form a time series. The resulting time series is displayed in figure 5.5.

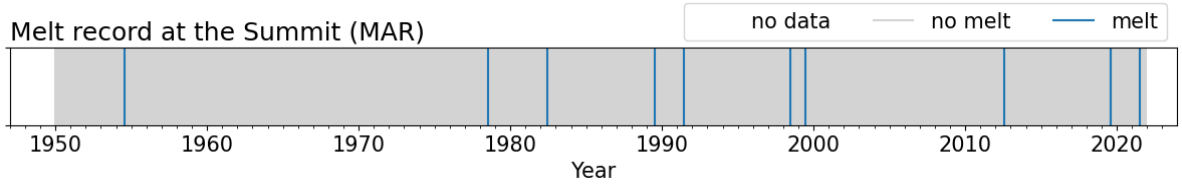

Figure C.5: Melt record at the Summit (MAR) (threshold = 6 pixels with 2.3 mm w.e. melt)

Event	Days	Year
1	14 July	1954
2	15 July	1978
3	8 June	1982
4	16 July	1989
5	18 June	1991
6	2 July	1998
7	28 June	1999
8	30 July	2012
9	30 - 31 July	2019
10	19 July	2021

Table C.8: Melt events in ERA forced MAR data (threshold = 6 pixels with 2.3 mm w.e. melt)

Data	Period	Probability Sep	Probability All
MAR	1950-2021	$\rightarrow 0$	1/7.1
	1990-2020	$\rightarrow 0$	1/6

Table C.9: Probability of melt occurring at the Summit. Based on ERA forced MAR data.

C.6. CESM HR results

The results of the melt event detection in the CESM HR data are presented here. Also, the results of the probability computations are described in this section. The CESM HR results are presented per time period, starting with the pre-industrial period, succeeded by the historical period and ending with projections for the future.

Pre-industrial (CTRL)

For the pre-industrial period, the detected melt events in all months are visualised in figure C.6. The control run (pre-industrial period) comprises five hundred years of data. In this timespan, four melt events are detected in total. Of these four melt events, no event occurred in September, therefore the melt record for September-melt events in the Control run is not shown. The four melt events in 500 years of data result in a probability of 1/125 (table C.10).

A time series of the pre-industrial period is constructed and is shown in figure 5.7 and figure 5.8.

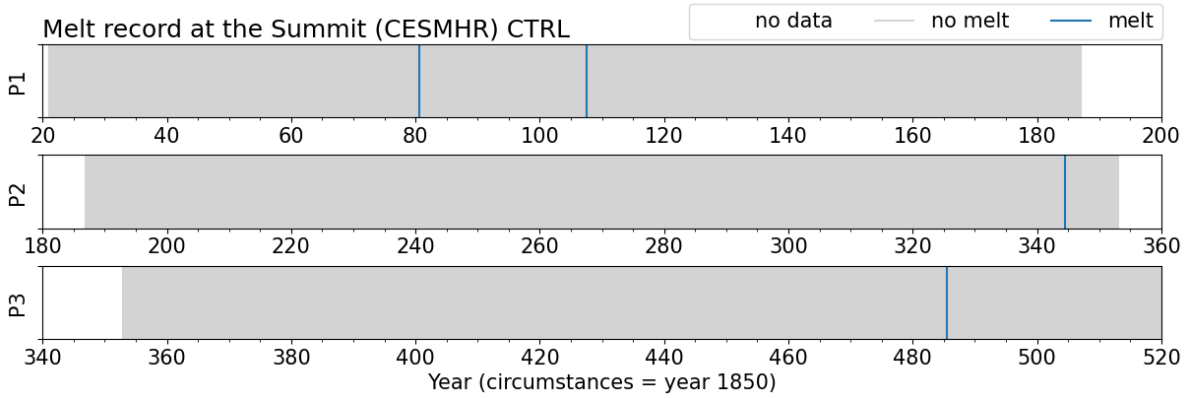

Figure C.6: Melt record at the Summit (CESMHR) CTRL. All months are taken into account. Threshold = one pixel with 3e-08 mm/s melt.

Data	Period	Probability Sep	Probability All
CESM HR E1	1850 (500 yr)	$\rightarrow 0$	1/125

Table C.10: Probability of melt occurring at the Summit in a climate like in 1850. Based on 500 years of CESM HR data.

Historical (HIST)

For the historical period, the detected melt events in all months are visualised in figure C.7 and the events detected in September are visualised in figure C.8. In the total time span of the ensemble members, eight, five and six melt events are detected between 1850-2021, 1920-2021 and 1920-2021 in E1, E2 and E3 respectively. Of these events, six, three and five events happened between 1990 and 2020. This results in probabilities 1/5, 1/7.5 and 1/6 for the three ensemble members, see table C.11.

When looking at the month of September in figure C.8, it strikes that two events are detected in two different ensemble members. This is more than in the observations altogether. Both the melt events fall within the 'current climate'-period. Due to the period of interest of 30 years, this results in probabilities 1/30, 1/30 and 0 respectively (see table C.11).

The probabilities are not only computed for the period of interest 1990-2020 but over the whole time span where data is available. The resulting time series is shown in figure 5.7.

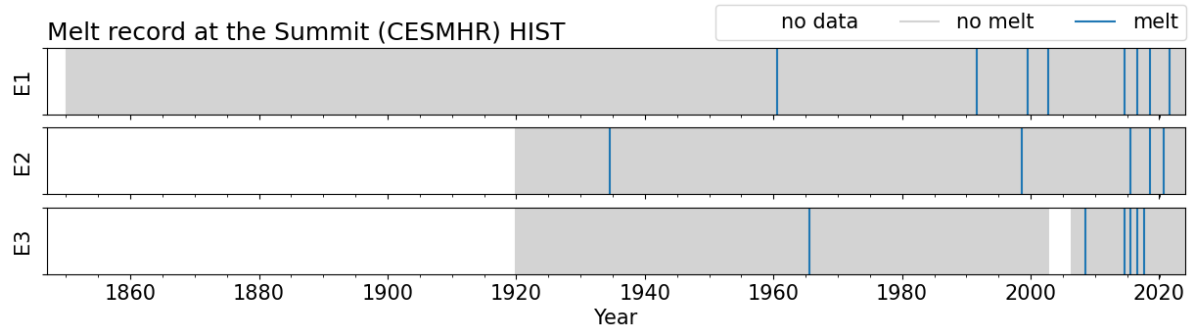

Figure C.7: Melt record at the Summit (CESMHR) HIST. Melt detected in any month is taken into account. A threshold of one pixel with 3e-8 mm/s is used for melt event detection.

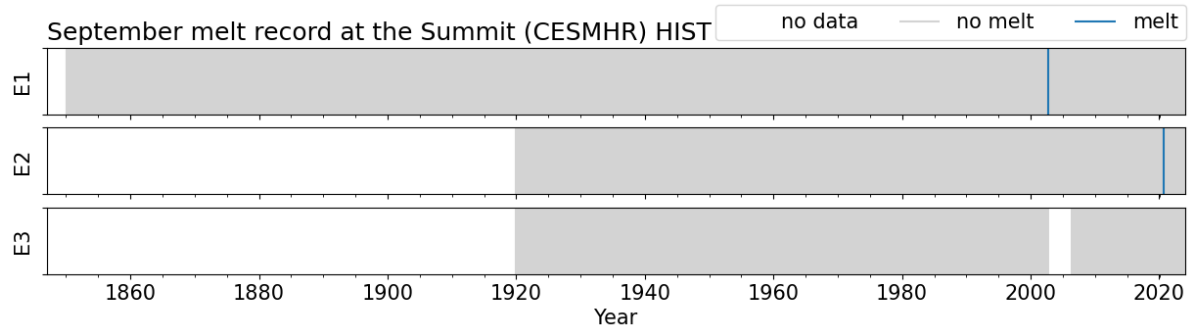

Figure C.8: September melt record at the Summit (CESMHR) HIST. A threshold of one pixel with 3e-8 mm/s is used for melt event detection.

Data	Period	Probability Sep	Probability All
CESM HR E1	1990-2020	1/30	1/5
CESM HR E2	1990-2020	1/30	1/7.5
CESM HR E3	1990-2020	$\rightarrow 0$	1/6

Table C.11: Probability of melt occurring at the Summit. Based on CESM HR data.

Future (FUT)

For the future period, the detected melt events in all months are visualised in figure C.9 and the events detected in September are visualised in figure C.10. The future simulations, here shown from 2021 to 2100, show an increasing amount of melt events toward the end of the century. From these melt events, quite some melt events happen in September. For the period 2070-2100, the probabilities per ensemble member are summarized in table C.12. The ensemble members show a probability of a year with melt in any month of 1/1.25, 1/1.3 and 1/1.07 at the end of the century, this means that approximately every year, melt occurs at the Summit. The probability of melt in September at the end of the century is, according to the three ensemble members, 1/2.14, 1/2.14 and 1/2.3. So every other year a melt event is expected to occur in September.

The probabilities change a lot between the beginning of the future simulation and the end of the simulation. The time series of these probabilities are displayed in figure 5.8 for all months as well as for September.

Data	Period	Probability Sep	Probability All
CESM HR E1	2070-2100	1/2.14	1/1.25
CESM HR E2	2070-2100	1/2.14	1/1.30
CESM HR E3	2070-2100	1/2.31	1/1.07

Table C.12: Probability of melt occurring at the Summit. Based on CESM HR data.

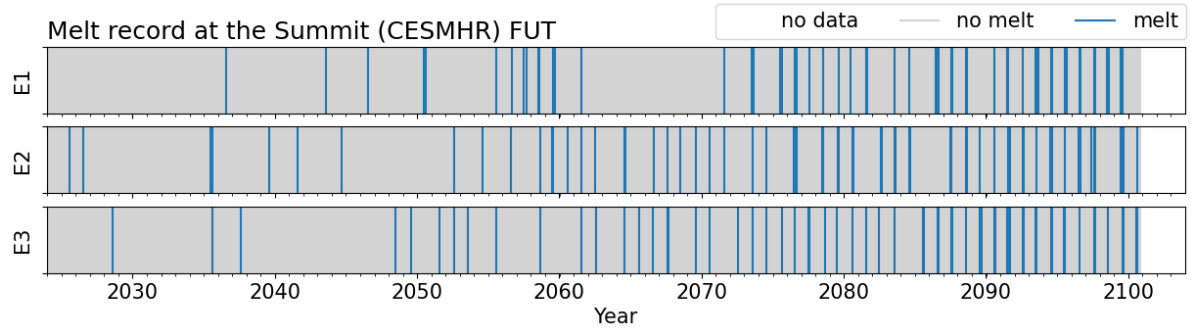

Figure C.9: Melt record at the Summit (CESMHR) FUT. All months are taken into account. Threshold = one pixel with 3e-08 mm/s melt.

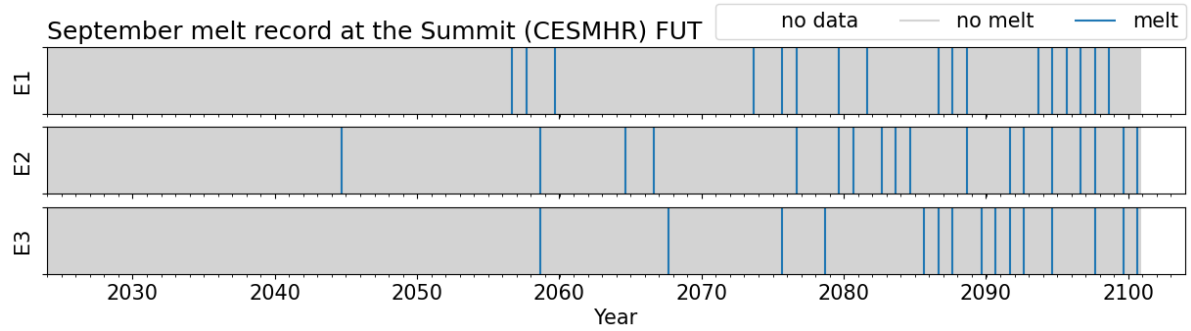

Figure C.10: September melt record at the Summit (CESMHR) FUT. Threshold = one pixel with 3e-08 mm/s melt.